Research Paper

GEOSPHERE

GEOSPHERE

https://doi.org/10.1130/GES02614.1

13 figures; 1 set of supplemental files

CORRESPONDENCE: john.grocott@durham.ac.uk

CITATION: Grocott, J., Thrane, K., McCaffrey, K.J.W., Sleath, P.R., and Dziggel, A., 2023, Andean-type, bivergent crustal shortening in the Rinkian orogen: New constraints on the tectonic evolution of Laurentia–West Greenland in the Paleoproterozoic: Geosphere, https://doi.org/10.1130/GES02614.1.

Science Editor: Andrea Hampel
Associate Editor: Robert B. Miller

Received 18 October 2022
Revision received 24 February 2023
Accepted 21 May 2023

Published online 27 July 2023

Andean-type, bivergent crustal shortening in the Rinkian orogen: New constraints on the tectonic evolution of Laurentia–West Greenland in the Paleoproterozoic

John Grocott[1], Kristine Thrane[2], Kenneth J.W. McCaffrey[1], Phoebe R. Sleath[1], and Annika Dziggel[3]

[1]Department of Earth Science, Durham University, Durham DH1 3LE, UK
[2]Geological Survey of Denmark and Greenland (GEUS), Øster Voldgade 10, 1350 Copenhagen K, Denmark
[3]Department of Tectonics and Resources, Institute of Geology, Mineralogy and Geophysics, Ruhr-Universität Bochum, Universitätsstraße 150, 44801 Bochum, Germany

ABSTRACT

The "Rinkian belt" of West Greenland is a metamorphic terrain of Paleoproterozoic age comprising: (1) the north Rinkian fold-thrust belt (FTB)—a pro- or fore-arc domain, highly deformed and metamorphosed with widespread anatexis; (2) the Prøven Igneous Complex—a magmatic arc characterized by hypersthene granitic rocks ("charnockites"); (3) the south Rinkian FTB—an inverted back-arc basin; and 4) a continental margin or foreland. Recognition of this tectonic architecture demonstrates that the "Rinkian" is a bona fide orogenic belt—the Rinkian orogen—and not simply the imbricated lower plate of the Nagssugtoqidian orogen. Arc plutons of the Prøven Igneous Complex were emplaced into the Karrat Group at ca. 1.90–1.85 Ga, dividing a back-arc basin into pro- and retro-arc domains. In the former—the north Rinkian FTB—WSW-directed thrusting (deformation events D_1-D_2) and high-grade metamorphism were taking place by ca. 1.875 Ga and were continuous through ca. 1.850 Ga with a peak temperature at ca. 1.830 Ma accompanied by anatexis in the Karrat Group and lower units of the Prøven Igneous Complex. In the retro-arc domain—the south Rinkian FTB—thrusting to the E (D_1) began at ca. 1.870 Ma followed by thrusting to the W (D_2) at ca. 1.830–1.820 Ga with displacement focused into a major high-temperature ductile shear zone which carried the Prøven Igneous Complex in the hanging wall of an Andean-type, crustal-scale, "pop-up" structure. High-temperature deformation continued during D_3 when the pro-arc, arc, and retro-arc domains were shortened by bivergent detachment folding and thrusting at ca. 1.820–1.810 Ga.

INTRODUCTION

The Rinkian belt is located north of the Nagssugtoqidian orogen in West Greenland and is exposed across 5° of latitude between Disko Bugt and Melville Bugt (Fig. 1A) (Grocott and Pulvertaft, 1990). It has a basement of Archean orthogneiss, with volumetrically minor amphibolite and paragneiss, overlain by late Neoarchean metasedimentary rocks of the Qeqertarssuaq Formation and Paleoproterozoic metasedimentary and metavolcanic rocks of the Karrat Group and the Anap nunâ Group (Escher and Burri, 1967; Escher and Pulvertaft, 1976; Henderson and Pulvertaft, 1967, 1987; Garde and Steenfeldt, 1999; Watt, 2019; Thrane, 2021; Guarnieri and Baker, 2022; Guarnieri et al., 2022a, 2022b, 2022c). The belt is divided into a north Rinkian fold-thrust belt (FTB) and a south Rinkian FTB by a large hypersthene granite—the Prøven Igneous Complex (PIC) (Fig. 1A) (Grocott and Pulvertaft, 1990; Thrane et al., 2005). The north Rinkian FTB—the focus of this paper—is a high-temperature metamorphic terrain, characterized by upper amphibolite to granulite facies grade rocks and widespread migmatization (Grocott and Pulvertaft, 1990). South of the PIC, although locally at granulite facies and accompanied by anatexis, metamorphic grade is generally much lower—at amphibolite to greenschist facies grade (Grocott and McCaffrey, 2017). The Karrat Group has been correlated with the Piling Group of the Foxe fold belt in Baffin Island (Nunavut, Canada) (Fig. 1B), and there are clear similarities in lithostratigraphy and structural style between the Foxe fold belt and the north Rinkian FTB (Henderson, 1981; Henderson et al., 1989; Hoffmann, 1999; Partin et al., 2014). Nevertheless, no plate tectonic model for the Trans-Hudson orogen explains how these belts were linked in a tectonic framework (Fig. 1C).

In central West Greenland, between Disko Bugt and the southern Nagssugtoqidian front at Kangerlussuaq (Fig. 1B), the plate tectonic model for the Nagssugtoqidian orogen and the south Rinkian FTB is better resolved (St-Onge et al., 2009). South-dipping subduction of oceanic lithosphere caused arc magmatism at ca. 1.92–1.87 Ga and was followed by continent-continent collision at ca. 1.85–1.82 Ga between the Rae and North Atlantic cratons to form the Nagssugtoqidian orogen with orogenic sutures recognized in the Disko Bugt region and at Nordre Strømfjord (Fig. 1B) (Kalsbeek et al., 1987; Connelly et al., 2000; van Gool et al., 2002; St-Onge et al., 2009; Garde and Hollis, 2010). In this scenario, the Rinkian FTB was envisaged to have formed by N-vergent thrust imbrication in the Rae craton, which comprised the lower plate of the Nagssugtoqidian orogen (Connelly and Thrane, 2005; Connelly et al., 2006; Grocott and McCaffrey, 2017). The PIC—in this model, a lower-plate granitic complex—was dated at ca. 1.87 Ga by Thrane et al. (2005), who found also

K.J.W. McCaffrey https://orcid.org/0000-0002-9882-1709

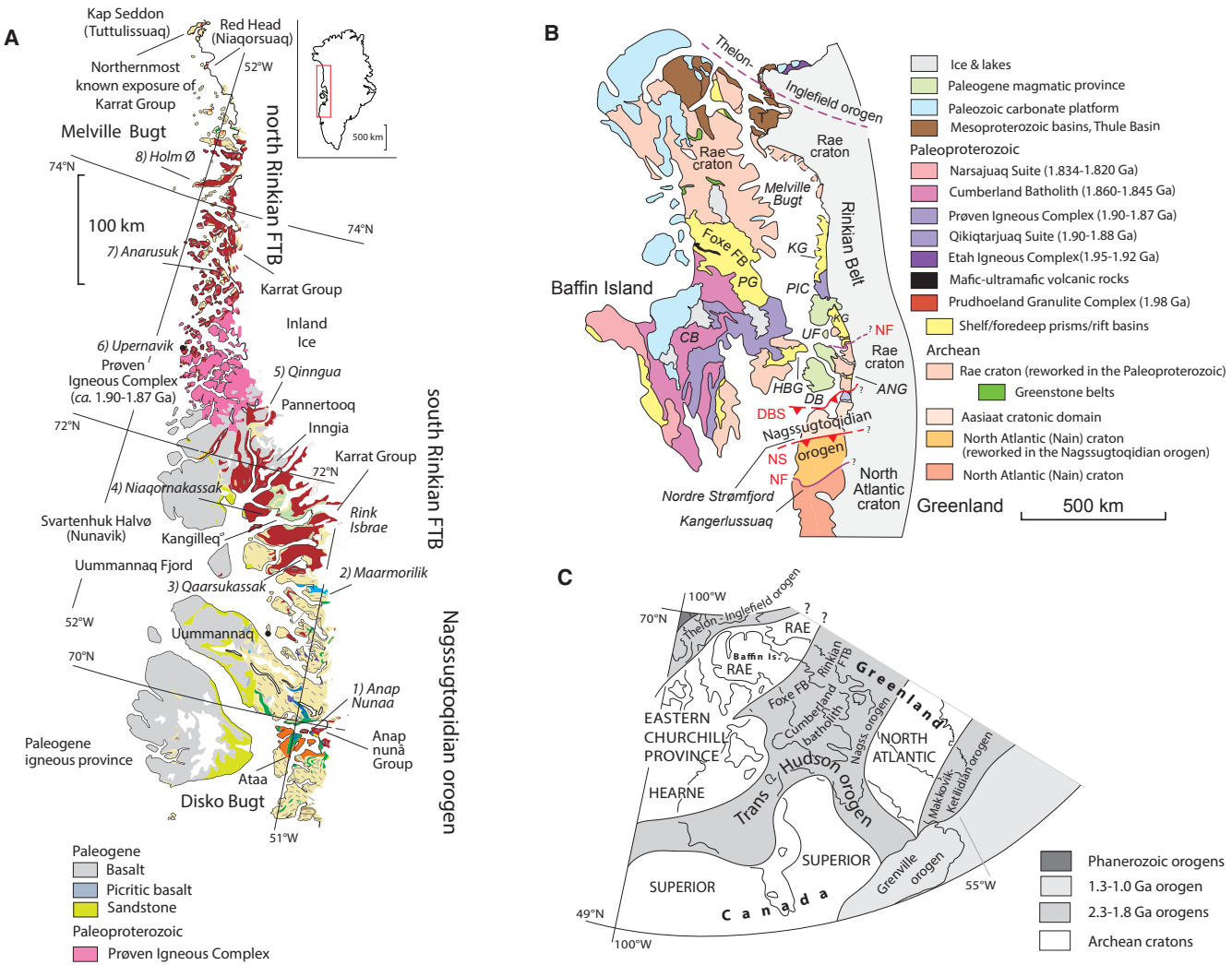

Figure 1. (A) Geology of central and northern West Greenland showing major rock units and location of the Nagssugtoqidian orogen and the Rinkian belt. Numbered localities correspond to stratigraphic columns in Figure 2. FTB—fold-thrust belt. Adapted from a map in the Geological Survey of Denmark and Greenland archives drawn by A.A. Garde. (B) Geology of central and northern West Greenland and Baffin Island (Canada) juxtaposed using the plate reconstruction of Lundin and Doré (2019). T—Thule basin; KG—Karrat Group; FB—fold belt; PG—Piling Group; PIC—Prøven Igneous Complex; UF—Uummannaq fjord; CB—Cumberland batholith; HBG—Hoare Bay Group; ANG—Anap Nuna Group; DB—Disko Bugt; DBS—Disko Bugt suture; NS—Nagssugtoqidian suture; NF—Nagssugtoqidian front (in Uummannaq Fjord, this is the northern limit of Nagssugtoqidian reworking of the south Rinkian FTB; Grocott and McCaffrey, 2017). Baffin Island geology after Sanborn-Barrie et al. (2017). (C) Map of the eastern Canadian Shield showing part of Paleoproterozoic supercontinent Laurentia and the upper (Churchill province) and lower (Superior craton) continental plates of the Trans-Hudson orogen and its extension into West Greenland (Lewry and Stauffer, 1990). Nagss.—Nagssugtoqidian. Redrawn after Sanborn-Barrie et al. (2017).

that it had geochemistry consistent with an A-type granite classification. They argued that magmatism of the PIC was generated during lithosphere delamination or rifting in the Rae craton, remote from the plate boundary, and it followed that no Paleoproterozoic suture, or former plate boundary, should exist within the Rinkian FTB. Recent petrological and geochemical work based on a much larger database compiled by the Geological Survey of Denmark and Greenland (GEUS) has led to reappraisal of PIC geochemistry showing that the complex largely comprises a suite of I-type granites likely to have formed in an upper-plate, continental magmatic arc setting (GEUS, 2022; Guarnieri et al., 2022d; T. Kokfelt, personal commun., 2023). An arc setting for the PIC is clearly not accommodated by current tectonic models at ca. 1.87 Ga for northern and central West Greenland and Laurentia (Van Kranendonk et al., 1993; St-Onge et al., 2009; Sanborn-Barrie et al., 2017).

We integrate recent and historic geological mapping with structural analysis and geochronology to compile a new map of the north Rinkian FTB. Field-based analysis of polyphase folding, mineral stretching fabrics, and kinematic indicators enables us to reconstruct deformation history and directions of tectonic transport. In addition, new U-Pb ages on zircon and monazite constrain the north Rinkian FTB in the orogenic evolution of northern West Greenland and Baffin Island.

STRATIGRAPHY

The distribution of the Karrat Group and the Anap nunâ Group has been used to define the Rinkian belt, placing the southern limit of the belt, and of the Rae craton, south of Anap Nunaa in northeastern Disko Bugt (Figs. 1 and 2) (Garde, 1994; Escher, 1995a; Garde and Steenfeldt, 1999; Connelly et al., 2006). Connelly and Thrane (2005) and Connelly et al. (2006) located the boundary at a high-strain zone south of the Atâ intrusive complex (Grocott and Davis, 1999), which St-Onge et al. (2009) and Garde and Hollis (2010) linked to exposures of ophiolitic rocks in the southern Disko Bugt region marking the Disko Bugt suture (Fig. 1B). In the north Rinkian FTB, metasedimentary rocks assigned to the Karrat Group are exposed at least as far north as Kap Seddon (Tuttulissuaq) (Fig. 1A) (Escher, 1981, 1983a, 1983b), but in this direction, the limit of the Karrat Group and of the Rinkian belt, is undefined.

South Rinkian FTB

An angular unconformity at the base of early Paleoproterozoic rocks is exposed in low-deformation areas close to the inland ice in the south Rinkian FTB between Rink Isbræ and northeastern Disko Bugt, where relatively weakly deformed Karrat Group and Anap nunâ Group rest on (mostly) polymetamorphic Archean gneiss (Figs. 1A and 2) (Garde and Pulvertaft, 1976; Henderson and Pulvertaft, 1987; Higgins and Soper, 1999; Nutman and Kalsbeek, 1999; Garde and Steenfeldt, 1999). In this domain, siliciclastic and carbonate rocks at the base of the Karrat Group with Pb-Zn mineralization have been assigned to the Qaarsukassak Formation (Guarnieri et al., 2016, 2022a, 2022b, 2022c; Watt, 2019) and correlated with the Mârmorilik Formation—a sequence of platform carbonates—exposed in the Uummannaq Fjord area (Figs. 1A and 2) (Garde, 1978; Henderson and Pulvertaft, 1987; Guarnieri and Baker, 2022). At its type section (Fig. 2), the Qaarsukassak Formation overlies the Archean Qeqertarssuaq Formation with angular unconformity in tilted extensional fault blocks and oversteps to rest on weakly deformed Archean gneiss (Guarnieri et al., 2022a). The Qaarsukassak Formation crops out more widely, albeit in areas of high Paleoproterozoic deformation where it has been interleaved with Qeqertarssuaq Formation (Sørensen and Guarnieri, 2018; Guarnieri et al., 2022b).

Detrital zircon age distributions in the Qaarsukassak Formation are dominated by late Archean ages, although a few zircon ages indicate an earliest Paleoproterozoic maximum depositional age (Guarnieri et al., 2022b). For the Qeqertarssuaq Formation, however, a minimum depositional age in the Paleoproterozoic (Sanborn-Barrie et al., 2017) has been re-evaluated in light of new data, and Rosa et al. (2017, 2018) argued that it was deposited in a basin of Neoarchean age—a precursor to the Karrat Group basin (Fig. 2). The dominant quartzite and quartz-arenite lithologies in both the Qeqertarssuaq and Qaarsukassak Formations may be indistinguishable in the field, and where deformation has erased the unconformity at the base of the Qaarsukassak Formation and interleaved the two formations, they are difficult to tell apart. Carbonate horizons in the Qaarsukassak Formation (Guarnieri et al., 2022b) may then be a useful lithostratigraphic criterion to distinguish it from the Qeqertarssuaq Formation.

The Qeqertarssuaq Formation and the Qaarsukassak Formation are interpreted to be syn-rift deposits laid down in late Neoarchean and early Paleoproterozoic time, respectively, during two tectonostratigraphic cycles (Guarnieri and Baker, 2022) in a system of half-graben basins controlled by normal-slip growth faults (Grocott and McCaffrey, 2017). These basins were overstepped by late- to post-rift basic volcanic rocks of the Kangilleq Formation (Fig. 2) (Henderson and Pulvertaft, 1987; Guarnieri et al., 2022b), which may mark a break-up unconformity (Grocott and McCaffrey, 2017). Turbidite-facies greywacke sandstone, siltstone, and shales of the Nûkavsak Formation (Fig. 2) then prograded across the rift basin architecture from the west ahead of an advancing thrust system—the Karrat Fjord thrust system (Grocott and McCaffrey, 2017)—an event signaled by change in provenance of detrital zircon grains in the Karrat Group (Kalsbeek et al., 1998; Sanborn-Barrie et al., 2017).

North Rinkian FTB

In the north Rinkian FTB, where the Karrat Group is dominated by rusty-weathered, high-grade paragneiss correlated with the Nûkavsak Formation (Figs. 3 and 4A), no angular unconformity at the base of the metasedimentary sequence has survived the deformation (Fig. 2) (Escher and Stecher, 1978, 1980; Grocott and Pulvertaft, 1990). Fabric intensity at the basement-cover

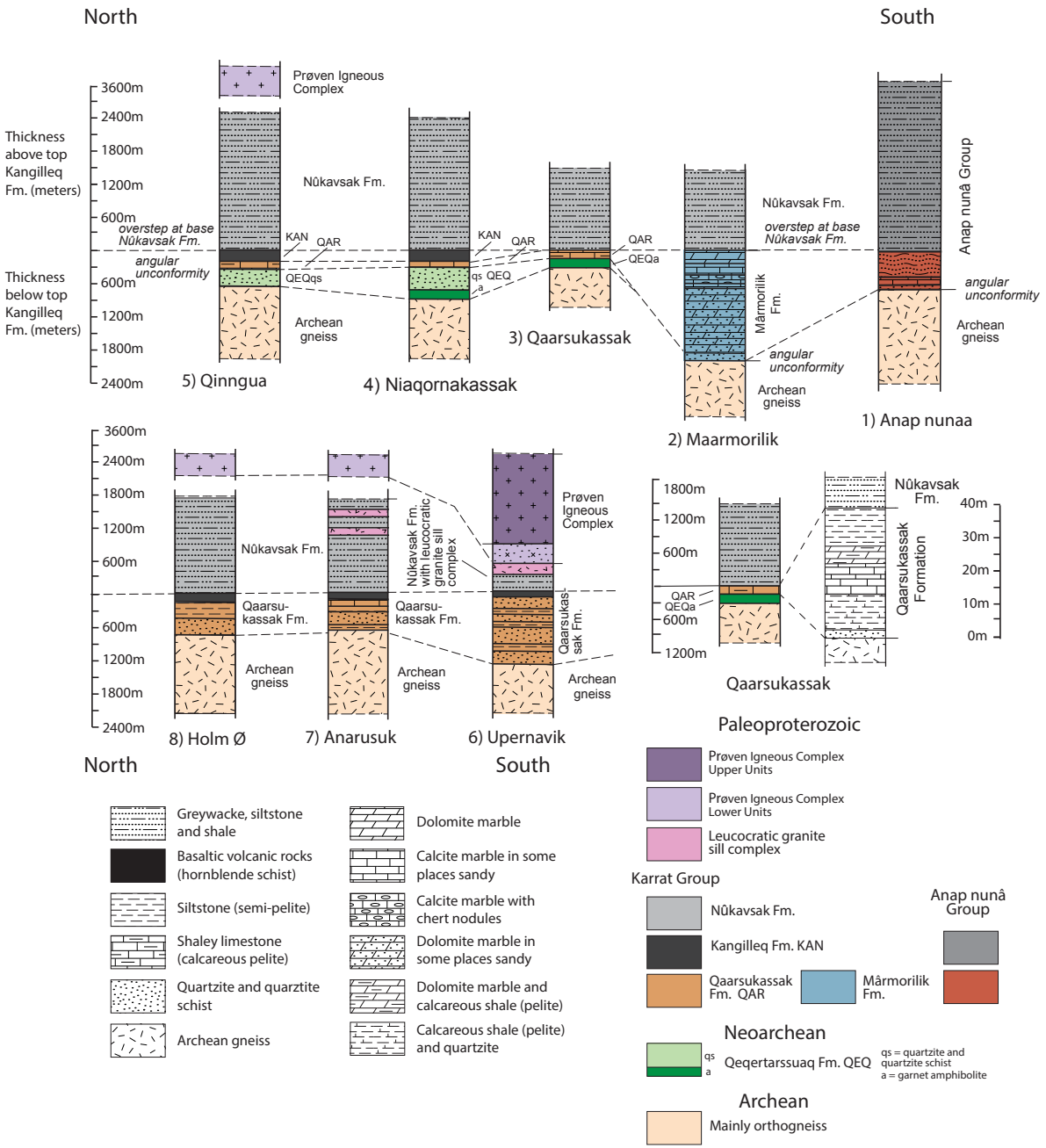

Figure 2. Lithostratigraphic columns for Paleoproterozoic metasedimentary sequences in the Rinkian orogen. These rocks are for the most part assigned to the Karrat Group, except in northeastern Disko Bugt where they are assigned to the Anap nunâ Group. At lower right, column 3 is expanded to show lithological detail for the Qaarsukassak Formation at the type section. Numbered locations of each stratigraphic column are shown in Figure 1A.

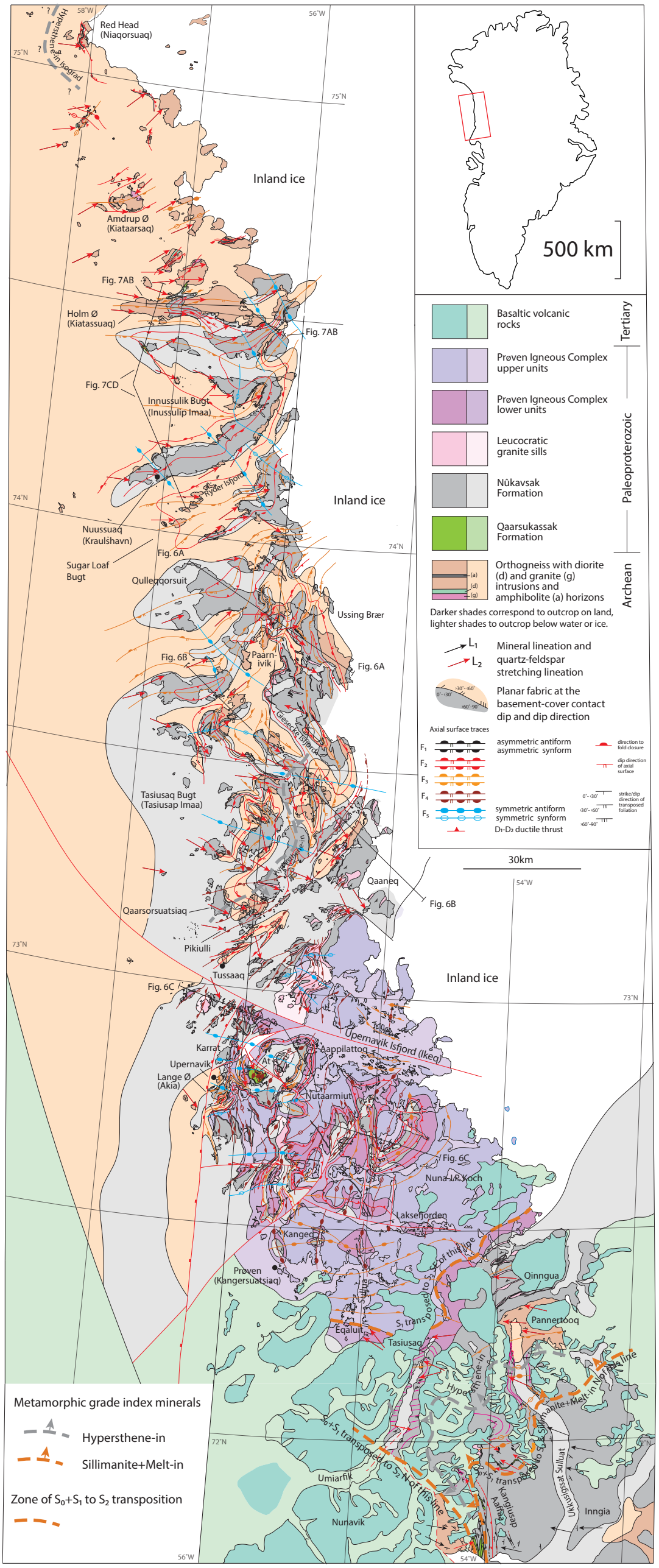

Figure 3. Structural geology of the northern Rinkian fold-thrust belt and the Prøven Igneous Complex (PIC) showing the axial surface traces of five fold phases, stretching lineations, orientation of the main planar fabrics, metamorphic index minerals, and the zone of $S_1 \rightarrow S_2$ transposition at the southern margin of the PIC. Positions of the cross sections in Figure 6 are shown. Atilissuaq is shown by the abbreviation At. Map is available in fully scalable digital format (.ai and .pdf) with additional structural layers—fold orientation, structural facing, and kinematic data—in the Supplemental Material (see text footnote 1).

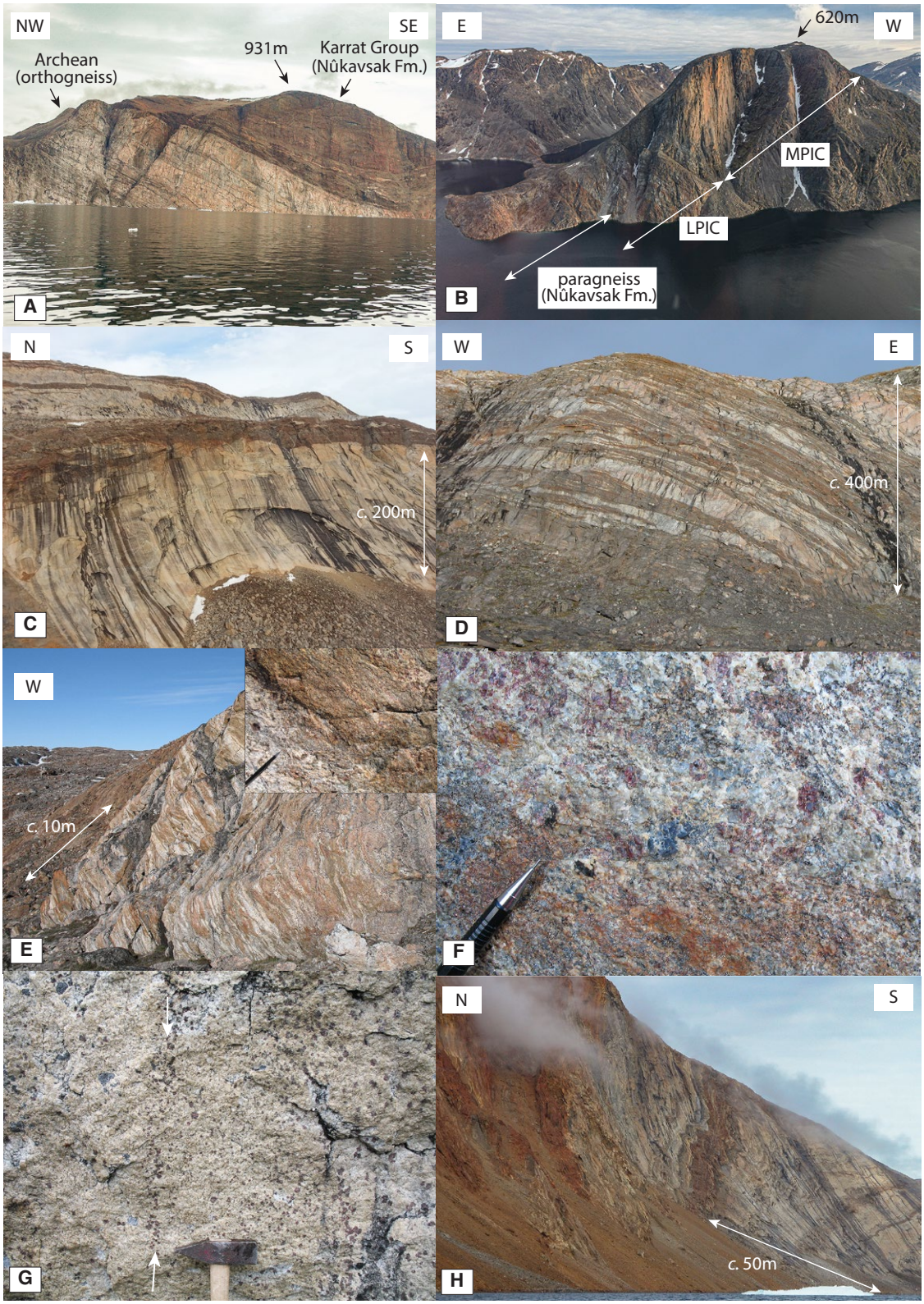

Figure 4. (A) Basement-cover contact east of Holm Ø (74°34.6′N, 56°23.3′W). (B) Lower contact of Prøven Igneous Complex (PIC) at Nutaarmiut (72°45.6′N, 55°55.7′W)—massive PIC (MPIC) overlies the thin, banded lower unit (LPIC) above rusty-weathered, banded, migmatitic paragneiss in the intrusion floor. (C) Leucocratic granite at sample site 567820 (73°36.9′N, 55°38.8′W)—main intrusion is massive and homogeneous; some apopheses in the paragneiss above are concordant, folded, and boudinaged in S_2-S_3 and others discordant and not deformed. (D) Leucocratic granite sill complex in the Tussaaq shear zone (at 73°18.4′N, 55°16.8′W)—sills are isoclinally folded and boudinaged in S_2-S_3-S_4, showing 30%–50% dilation of the host paragneiss. (E) Diffuse (mingling) contacts between paragneiss diatexite and leucocratic granite at 72°50.4′N, 56°5.0′W, on Karrat. (F) Garnet-cordierite-quartz-feldspar leucosome in diatexite paragneiss at 72°50.4N, 56°5.0′W, on Karrat. (G) Peritectic garnet defining former bedding trace—indicated by the vertical trail of garnet grains between the white arrows at 72°39.7′N, 54°48.9′W, on Nuna JP Koch. (H) Folded D_1 thrust sheets, northern limb of a major F_3 fold, eastern Inussulik Bugt (74°19.6′N, 56°21.1′W).

contact is high everywhere, and the rocks are migmatitic at least as far north as Kap Seddon—metatexite in the north and diatexite closer to the PIC —and they are in granulite facies for 30–60 km north of the PIC contact and again at Red Head (Niaqorsuaq) (Grocott and Pulvertaft, 1990) (migmatite terminology from Sawyer, 2008). Elsewhere, they are in upper amphibolite facies with sillimanite-bearing metatexite exposed across large tracts of ground (Fig. 3). The paragneiss oversteps a unit comprising quartzite, quartz arenite, marble, calc-silicate, carbonate, amphibolite, and ultrabasic rocks with a preserved thickness of a few meters to >1 km near Upernavik (Figs. 2 and 3) (Escher and Stecher, 1980). This was correlated with the Qeqertarssuaq Formation during 1:100,000-scale and 1:500,000-scale survey mapping (Escher 1981, 1983a, 1983b, 1995b), although carbonate rocks in the sequence point to correlation with the Qaarsukassak Formation (Guarnieri et al., 2022b, 2022c).

PRØVEN IGNEOUS COMPLEX (PIC)

The PIC comprises a suite of hypersthene granites—"charnockites"—that underlies an area of at least 7200 km^2 in the central part of the Rinkian FTB (Fig. 3) (Escher and Pulvertaft, 1976; Escher and Stecher, 1978; Grocott and Pulvertaft, 1990; Thrane et al., 2005; T. Kokfelt, personal commun., 2023). The base is in contact with migmatitic paragneisses, correlated with Nûkavsak Formation and metamorphosed at granulite facies grade, that dip below the lower contact (Fig. 4B) (Henderson and Pulvertaft, 1987; Grocott and Pulvertaft, 1990). The complex lies above its host rocks with its "floor" defining a sub-horizontal envelope. It is presumed that it has a sheet-like or tabular shape and the roof has been removed by erosion (Sleath, 2021).

When Grocott and Pulvertaft (1990) published a review of the Rinkian belt, the only geochronology for the PIC was a Rb-Sr whole-rock isochron age of 1860 ± 25 Ma (Kalsbeek, 1981). Later, Thrane et al., (2005) determined a U-Pb sensitive high-resolution ion microprobe (SHRIMP) age of 1869 ± 9 Ma, refining the Rb-Sr result. The much larger database of U-Pb data now available shows that the complex was emplaced over ~50 m.y. and comprises three intrusive suites emplaced at ca. 1900 Ma, ca. 1870 Ma, and ca. 1850 Ma (Sanborn-Barrie et al., 2017; GEUS, 2022; T. Kokfelt, personal commun., 2023).

LEUCOCRATIC GRANITE INTRUSIONS

Leucocratic granite sills, some of them kilometer-thick tabular intrusions, dikes, and veins, intrude migmatitic paragneisses below the PIC and the lower part of the PIC (Fig. 4C). The sill complex is exposed at the margins of the PIC and in erosional windows into the floor of the PIC as far east as Nuna J.P. Koch (Fig. 3). Leucocratic granite sills are also exposed between Qaaneq and Ussing Brær, close to the ice margin, and parallel to the presumed northward continuation of the PIC below inland ice (Fig. 3). The thickest sills were emplaced in the uppermost 2–3 km of paragneiss below the lower contact of the PIC, where they comprise 30%–50% of the rock volume (Fig. 4D). The spatial relationship between leucogranite intrusions and the hypersthene granite complex is so close that previous authors assumed that they were all a component of PIC magmatism (Escher and Stecher, 1980; Grocott and Pulvertaft, 1990).

Diatexite migmatites crop out over a wide area north of the PIC (Fig. 3) and are characterized by soft or diffuse contacts between migmatitic metasedimentary rock (Fig. 4E) and (commonly) garnet- and (rarely) cordierite-bearing leucosomes (Fig. 4F). These in-source leucogranites commonly contain trails of peritectic garnet that mark relict bedding. They are clearly more-or-less in situ melts (Fig. 4G). Therefore, although some leucogranite intrusions may represent components of PIC magmatism, many are leucosomes derived by partial melting of paragneiss and extracted from the paleosomes during deformation to form intrusive, but nevertheless in-source, leucogranites (Rosa et al., 2018).

METHODS AND DATA

Interpretation of structure and kinematics in the north Rinkian FTB is based on a compilation of GEUS mapping (Escher, 1981, 1983a, 1983b, 1995a) plus ship-based fieldwork to gather data on attitude and superposition of folds and the orientation and nature of planar and linear deformation fabrics. Field data were collected digitally with direct input into ArcGIS. The outcome is a new, scalable structural map compilation for the north Rinkian FTB, including the offshore areas between Upernavik (72°45′N) and Kap Walker (75°40′N), drawn at a nominal scale of 1:100,000 (Fig. 3) (File S1 in the Supplemental Material[1]). The structural map of the PIC was compiled from 1:40,000-scale unpublished field maps held in archives at GEUS (Pulvertaft et al., 1979) and new photogrammetric data (Sørensen and Dueholm, 2018; Sleath, 2021). This was supplemented by data collected during helicopter-supported fieldwork linked to systematic mapping by GEUS and merged with the structural map of the north Rinkian FTB (Fig. 3; File S1).

RESULTS FROM STRUCTURAL ANALYSIS

Red Head (Niaqorsuaq) to Upernavik

Deformation Events D_1-D_2

Basement Archean orthogneisses were interleaved with their Paleoproterozoic metasedimentary cover by thrusting during the first regional deformation

[1]Supplemental Material. File S1: Structural map for the north Rinkian FTB, the PIC, and the south Rinkian FTB on Nunavik (Svartenhuk Halvø) and Inngia; file contains structural data layers additional to Figure 3 (Adobe layered .pdf file). File S2: Analytical methods (.pdf file). File S3: Table S1, U-Th-Pb data from zircons (.xlsx file). File S4: Table S2, U-Th-Pb data from monazites (.xlsx file). Please visit https://doi.org/10.1130/GEOS.S.23483105 to access the supplemental material, and contact editing@geosociety.org with any questions.

in the north Rinkian FTB (D_1) (Fig. 4H). Thrust sheets are characteristically a few meters to a few hundred meters thick with high aspect ratios, so they can be traced many kilometers along strike (Pulvertaft, 1973, 1986). Examples of D_1 thrust imbrication are exposed at Nuussuaq, Inussulik Bugt (Inussulip Imaa), Holm Ø (Kiatassuaq), and farther north at Red Head (Niaqorsuaq) (Fig. 3). The earliest planar fabric in metasedimentary rocks of the Karrat Group is bedding (S_0) which, nearly everywhere, was transposed to differentiated lithological layering ($S_0 + S_1$) during D_1. Where D_1 fabric intensity is low, for example at Qaarsorsuatsiaq (Fig. 3), quartz-feldspar-biotite-garnet neosome in sheet silicate-rich S_1 cleavage domains oblique to S_0 shows that partial melting started during D_1, under upper amphibolite facies conditions (Fig. 5A).

A system of large-scale fold nappes is highlighted by the basement-cover contact north of the PIC (Figs. 3, 5B, and 6; File S1, footnote 1) (Escher 1981, 1983a, 1983b). The nappes are close to isoclinal, recumbent, F_2 folds of the basement-cover contact, D_1 thrust sheets, and D_1 planar and linear fabrics ($S_0 + S_1$ and L_1). A cross section at a high angle to the ENE-plunging regional stretching lineation in the Holm Ø–Nuussuaq district reveals closed—eye-shaped—patterns in the basement-cover contact in a complex pattern of superposed folding (F_2-F_3-F_5) (Fig. 7). In limbs of F_2 folds, bedding (S_0) and D_1 planar and linear fabrics (S_1, L_1) have been transposed ($S_0 + S_1 \rightarrow S_2$) ($L_1 \rightarrow L_2$) (Fig. 5B). The orientation of the transposed planar fabric (S_2) is variable due to superposed folding, but on average, it has NNE (010°) strike and 23°ESE dip (Fig. 8A). Northwest of Tasiusaq Bugt (Tasiusap Imaa) and Ussing Brær (Fig. 3), the lineation (L_2) has a W to WSW trend with an average plunge direction of 086° and an average plunge of 39° (Figs. 8A and 8B). Therefore, the direction of ductile flow during D_2 was W-E in a gently E-dipping shear plane, almost perpendicular to the present-day coastline. South of Tasiusaq Bugt (Tasiusap Imaa), L_2 has been bent around large-scale, late, open folds, and the link to transport direction is less clear-cut (Figs. 3, 8B, and 8C). In common lithologies—orthogneisses and siliciclastic metasedimentary rocks—planar fabrics ($S_0 + S_1 \rightarrow S_2$) are defined by quartz-feldspar shape fabrics and biotite mineral fabrics, with the flattening plane parallel to differentiated lithological layering (Fig. 5C). The lineation ($L_1 \rightarrow L_2$) (Fig. 5D) is a quartz or quartz-feldspar shape fabric and/or a mineral lineation defined by biotite, hornblende, and, in pelitic rocks, sillimanite (Grocott and Pulvertaft, 1990).

Switches in the direction of structural facing along the axial surface trace of F_2 folds show that they are sheath-like with highly non-cylindrical hinge lines (Fig. 7). We interpret this to mean that as F_2 folds amplified into sheath folds, from initially more cylindrical folds oriented at a high angle to the transport direction, their hinge lines rotated toward the D_2 transport direction defined by the regional lineation (L_2) (Fig. 8D). Consequently, high angles between F_2 fold hinges and the regional stretching lineation (L_2) remain only in sheath fold culminations and depressions (Fig. 7). By way of analogy, vergence and facing patterns of F_2 fold nappes of the north Rinkian FTB are comparable to those of the Neoproterozoic Moine nappe in the Caledonian orogen of northern Scotland (Alsop and Holdsworth, 1999, 2002, 2004).

Foliation ($S_0 + S_1 \rightarrow S_2$) associated with the regional stretching lineation ($L_1 \rightarrow L_2$) contains ubiquitous, large- and small-scale asymmetric porphyroclast systems and asymmetric boudins of quartz and granitic veins and lenses (Figs. 3 and 5E). Asymmetry of kinematic indicators shows that deformation during D_2 was non-coaxial and the sense of regional tectonic transport during D_2 was top-to-the-W. Transposition of D_1 fabrics during D_2 has overprinted evidence for the sense of tectonic transport during D_1.

Superposition of Folds of Deformation Events F_2-F_3

Interference between gently inclined to recumbent N-S–trending sheath folds (F_2) and E-W–trending moderately inclined folds (F_3) has produced a Ramsay type 2 (Ramsay and Huber, 1987; dome-crescent-mushroom) superposed fold pattern (Fig. 3). The earlier phase of folding, F_2, had sheath-like form *before* the later phase folds, F_3, were superimposed (Fig. 7). The fold superposition pattern is particularly clear between Holm Ø (Kiatassuaq) and Qulleqqorsuit but is present throughout the area, including south of a line between Tasiusaq Bugt and Ussing Isbræ where later deformation phases, D_4 and D_5, were superimposed more strongly on the F_2-F_3 pattern (Figs. 3 and 9).

Hinge lines of F_3 plunge gently E or ENE in a similar direction to the regional mineral stretching lineation (L_2) (Fig. 8D). The coaxial characteristics of F_2 sheath fold hinge lines, F_3 fold hinge lines, and the regional mineral stretching lineations may imply that D_2-D_3 were progressive. However, in the Holm Ø–Nuussuaq area, axial surfaces of F_2 and F_3 folds have almost perpendicular trends (Fig. 3). More likely, then, the direction of shortening changed from approximately E-W (D_1-D_2) to NW-SE or even N-S during D_3.

Intrusions in the leucocratic granite sill complex, exposed between Qaaneq and Ussing Brær, were folded isoclinally by F_2 and F_3 with extreme boudinage in highly attenuated, isoclinal F_2 fold limbs (Escher, 1983a) (Figs. 3, 4D, 6A, and 6B). Nevertheless, crystal-plastic shape fabric intensity in the sills is weak due to high-temperature annealing, and internally, larger intrusions may appear undeformed (Fig. 4C).

Tussaaq Shear Zone (Deformation Event D_4)

The Tussaaq shear zone is a 6–8-km-wide, NE-trending, high-fabric-intensity belt at the northern and western margins of the PIC (Fig. 9) (Grocott and Pulvertaft, 1990) in which the base of the PIC and underlying hypersthene-bearing migmatitic paragneisses and leucocratic granitic sills have been folded and reworked (Figs. 6B and 6C). In general, metamorphic grade is at granulite facies, although at some exposures, the fabric is porphyroclastic and recrystallized under amphibolite facies conditions, implying that the Tussaaq shear zone accommodated deformation down to lower temperature (Rosa et al., 2016, 2017, 2018). The regional mineral stretching lineation (L_1-L_2) was rotated and intensified to a new (transposed) lineation in the Tussaaq shear zone, with a mean plunge of 45° to 140° and a steep pitch in the foliation (Figs. 8B and 8E). The F_2-F_3 fold interference pattern was flattened and rotated into the shear

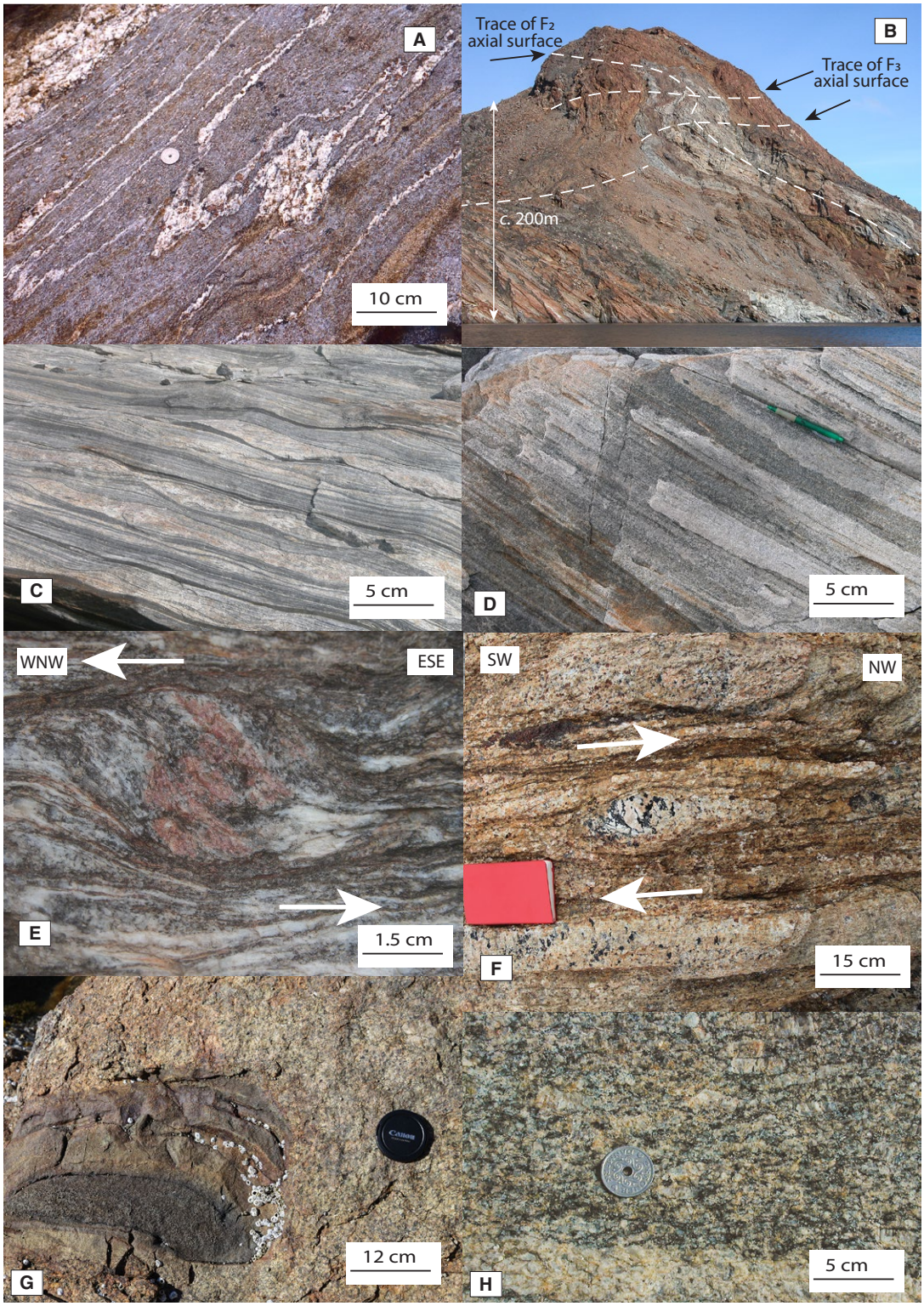

Figure 5. (A) Granite leucosome in S_1 migmatized cleavage domains, Pikiulli (73°7.53′N, 56°11.5′W). (B) Isoclinal F_2 fold at Ryder Isfjord (Nuussuaq kangia) (74°3.9′N, 56°20.9′W). Archean orthogneiss (gray) is exposed in the fold core, and the fold envelope is formed from Paleoproterozoic paragneiss (Nûkavsak Formation). In the orthogneiss, the folded differentiated (compositional) layering is S_1, and in the metasedimentary rocks, the folded layering is S_0 transposed to, and parallel with, S_1. In the isoclinal fold hinge, S_2 is in the fold axial plane and has crenulated S_1 and $S_0 + S_1$, but in the fold limbs, all planar fabrics were transposed to S_2 ($S_0 + S_1 \rightarrow S_2$) as seen in the inverted limb in the left foreground. (C) Differentiated (compositional) layering in orthogneiss, Kap Seddon (Tuttulissuaq) (75°24.1′N, 58°19.4′W). (D) Stretching fabric defined by quartz-feldspar aggregates parallel with an intersection lineation (S_0+S_1xS_2) in orthogneiss, Kap Seddon (Tuttulissuaq) (75°24.1′N, 58°19.4′W). (E) Asymmetric plagioclase rim on garnet, Red Head (75°4.6′N, 58°5.2′W). Exposure surface is perpendicular to the foliation ($S_0 + S_1 + S_2$) and parallel to the regional stretching lineation ($L_1 + L_2$), which indicates transport direction. (F) Asymmetric orthoclase feldspar porphyroclast, kinematic indictor for top-to-the-NW shear sense in the Prøven Igneous Complex (PIC), Atilissuaq (72°47.0′N, 55°.55.6′W). (G) Metasedimentary inclusions in the PIC, Aappilattoq (72°51.1′N, 55°32.5′W). (H) Orthoclase phenocrysts in the upper, massive unit of the PIC unit defining a magmatic state fabric, north of Tasiusaq (72°15.3′N, 54°23.1′W).

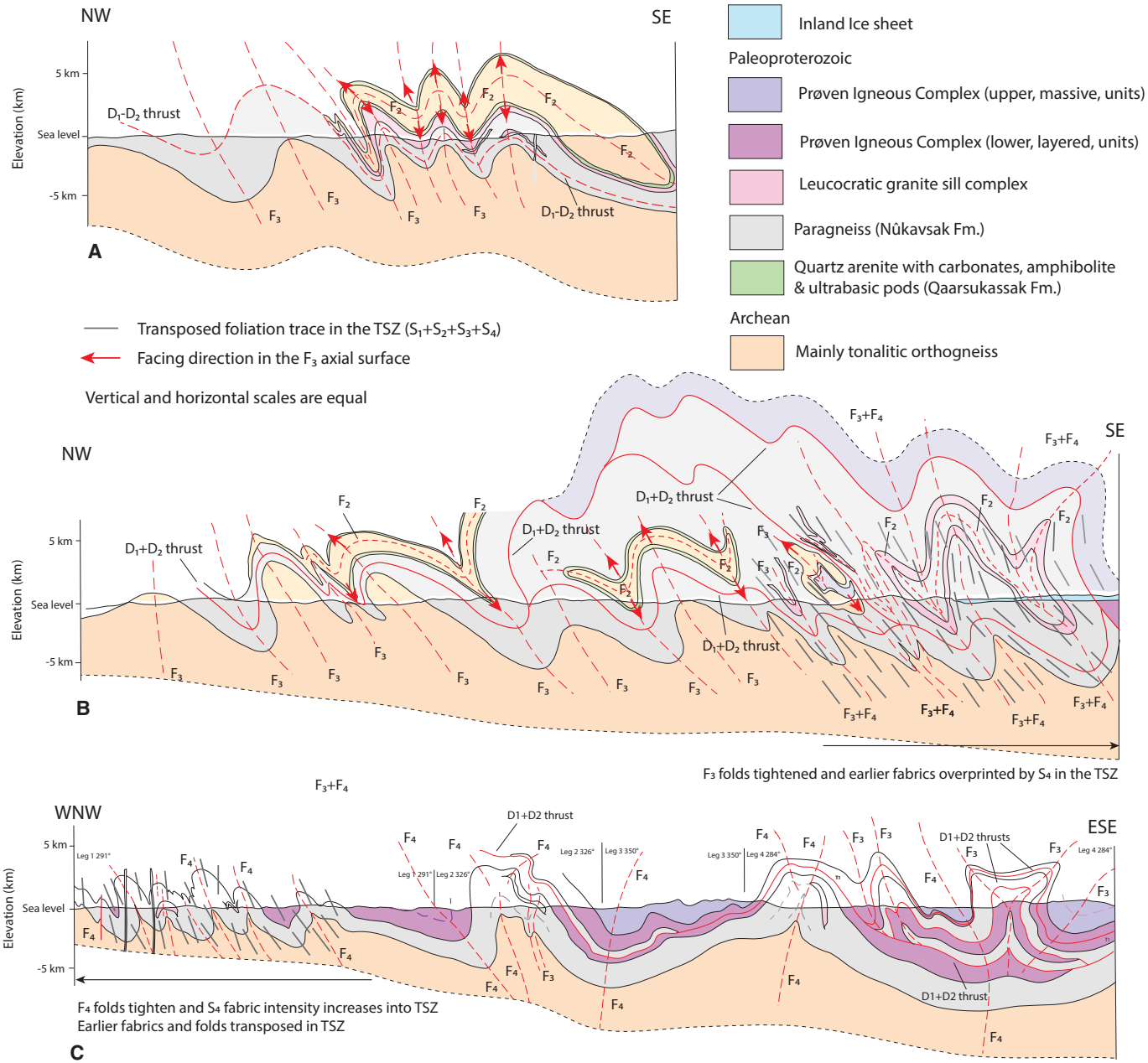

Figure 6. Cross sections through the northern Rinkian fold-thrust belt. (A) Ussing Isfjord. (B) Giesecke Isfjord to the northern boundary of the Prøven Igneous Complex at Qaanaq. (C) Upernavik Isfjord to Nuna J.P. Koch. Lines of the sections are shown on Figure 3. In sections (A) and (B), colors are faded above the topographic line to differentiate interpretation above and below the ground surface, respectively. On section line (C), the position where the line changes trend are shown on Figure 3. TSZ—Tussaaq shear zone.

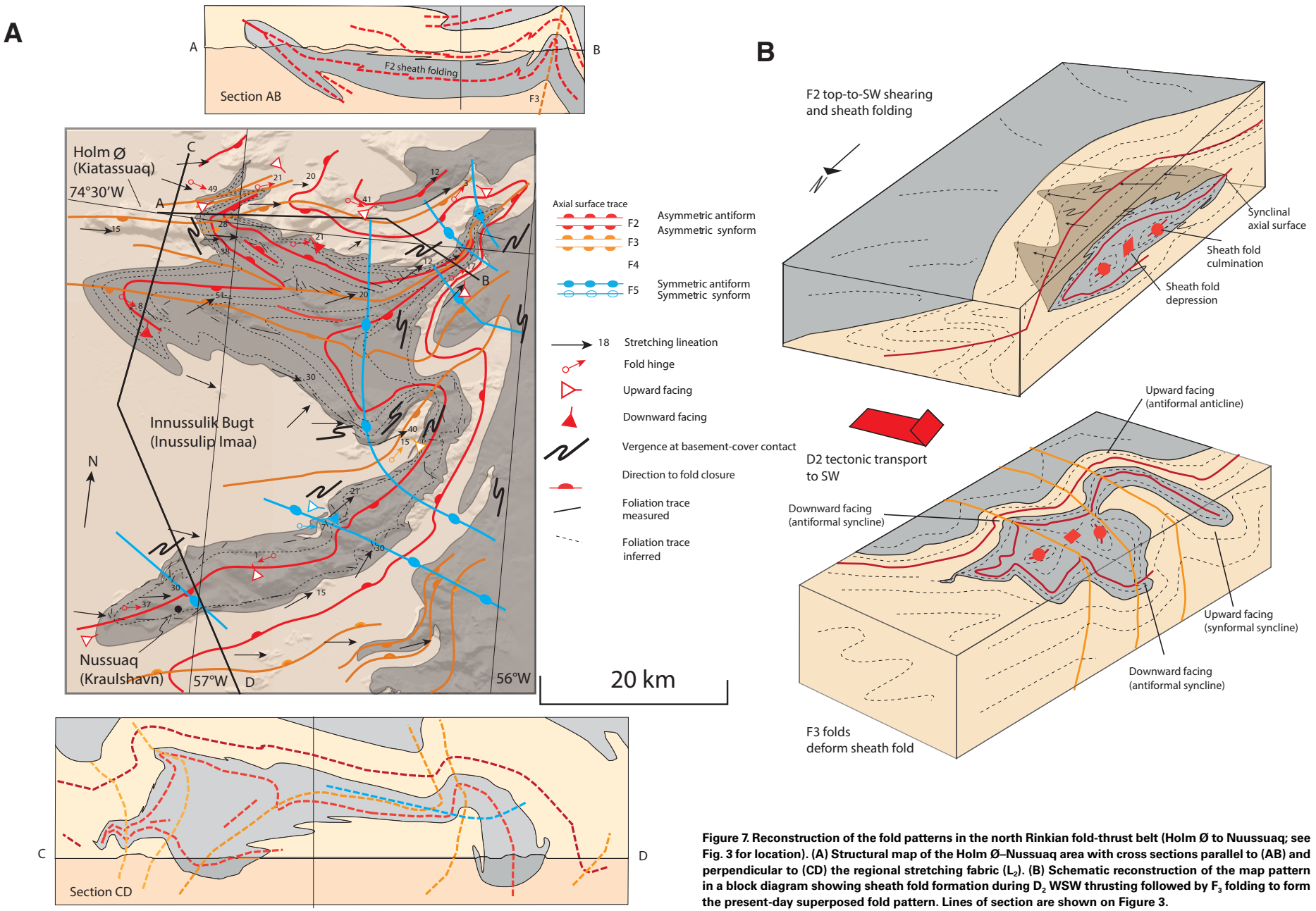

Figure 7. Reconstruction of the fold patterns in the north Rinkian fold-thrust belt (Holm Ø to Nuussuaq; see Fig. 3 for location). (A) Structural map of the Holm Ø–Nussuaq area with cross sections parallel to (AB) and perpendicular to (CD) the regional stretching fabric (L_2). (B) Schematic reconstruction of the map pattern in a block diagram showing sheath fold formation during D_2 WSW thrusting followed by F_3 folding to form the present-day superposed fold pattern. Lines of section are shown on Figure 3.

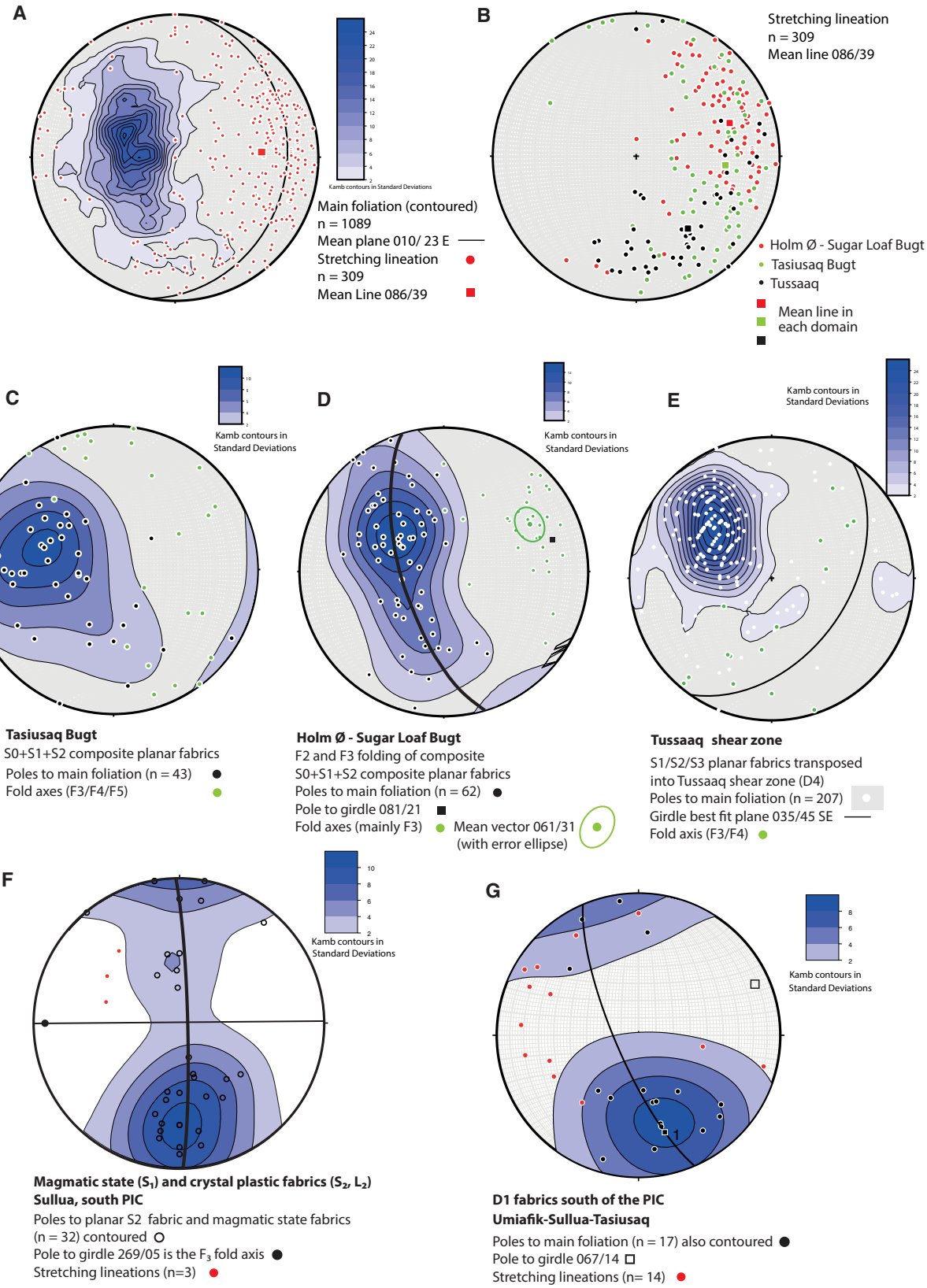

Figure 8. Stereographic projections of orientation data in the north Rinkian fold-thrust belt. (A) Poles to the main planar fabric ($S_0 + S_1 + S_2$) and plunge and plunge directions of the shape and mineral fabrics (stretching fabrics) ($L_1 + L_2$) north of the Prøven Igneous Complex (PIC). (B) Shape and mineral fabrics (stretching fabrics) ($L_1 + L_2$) subdivided by area north of the PIC. (C) Composite planar fabrics ($S_0 + S_1 + S_2$), Tasiussaq Bugt. (D) F_2 and F_3 folds of composite planar fabrics ($S_0 + S_1 + S_2$), Holm Ø to Sugarloaf Bugt. (E) $S_0 + S_1 + S_2$ fabrics transposed to S_4 in the Tussaaq shear zone. (F) Magmatic state planar fabrics (S_1) and crystal-plastic fabrics (S_2) (L_2), south PIC at Sulluat. Pole to the best-fit great circle to planar data gives the F_3 fold axis. (G) Planar ($S_0 + S_1 + S_2$) and linear ($L_1 + L_2$) fabrics in the Nûkavsak Formation, south side of the PIC at Umiarfik-Sullua-Tasiusaq. Pole to the best-fit great circle to planar data gives the F_3 fold axis.

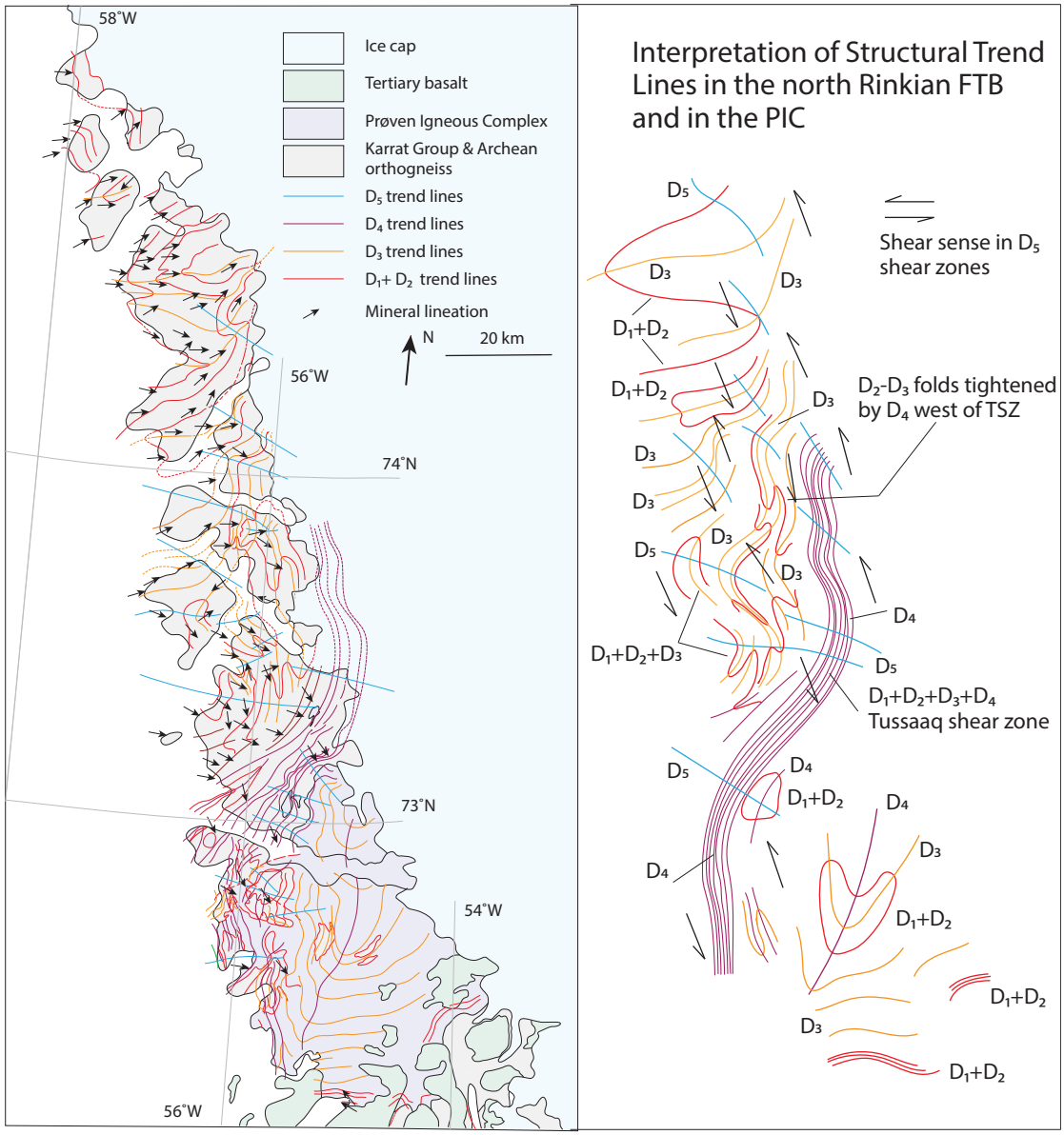

	North Rinkian FTB & western PIC			South Rinkian FTB & eastern PIC		
D_1	Ductile thrusts - vergence uncertain	Upper amphibolite facies metatexite	Begins at *ca.* 1900 Ma	ESE-vergent ductile thrusts	Upper amphibolite to granulite facies	Begins at *ca.* 1900 Ma
D_2	WSW-vergent ductile thrusts	Upper amphibolite to granulite facies diatexite	*ca.* 1875 - 1820 Ma	WSW-vergent ductile thrusts	Upper amphibolite to granulite facies diatexite	*ca.*1870 - 1830 Ma
D_3	NW-SE shortening, NW-vergent folds	Amphibolite facies	*ca.* 1820 - 1810 Ma	N-S shortening, S-vergent folds	Amphibolite facies	< *ca.*1830 Ma > *ca.* 1810 Ma
D_4	NW-vergent ductile thrusts & folds	Amphibolite facies	*ca.* 1820 - 1810 Ma	Not present		
D_5	Dextral heterogeneous simple shear	Amphibolite facies	<1810 Ma	Not present		

Figure 9. Trend surface map showing trends and relative age of the planar fabrics in the north Rinkian fold-thrust belt (FTB) and in the Prøven Igneous Complex (PIC) (foliation and fold axial surface traces). Simplified map to the right highlights the position of the Tussaaq shear zone (TSZ) (D_4) and the shear sense of the main D_5 zones of heterogeneous sinistral simple shear.

zone, and planar fabrics ($S_0 + S_1 + S_2 + S_3$) were transposed into a new foliation ($S_0 + S_1 + S_2 + S_3 \rightarrow S_4$), in the shear zone. Therefore, the Tussaaq shear zone is a D_4 structure (Fig. 9). Kinematic indicators may show ambiguous or conflicting asymmetry, but most, including those in zones of reworking at lower metamorphic grade, are consistent with top-to-the-NW displacement implying reverse slip during D_4 (Fig. 5F).

Superimposed Heterogeneous Ductile Shear (Deformation Event D_5)

The F_2-F_3 fold interference pattern has been flattened and rotated in NW- to NNW-trending zones of superimposed sinistral heterogeneous ductile shear (Fig. 9). This caused large-scale, open folding of the F_2-F_3 fold interference pattern (D_5), especially southeast of Ussing Brær and Tasiusaq Bugt, where axial surface traces of F_2-F_3 folds and the stretching lineation (L_2) were reoriented in zones of heterogeneous ductile shear expressed as open folds (F_5) (Figs. 3 and 8B).

Prøven Igneous Complex

Northern and Western Margins

In the PIC, six lithostratigraphic and igneous units were recognized (Figs. 2, 3, and 6C) (Sleath, 2021): (1) orthogneiss—now metatexite to diatexite migmatite (Archean; last migmatized in the Paleoproterozoic); (2) quartz arenite with minor marble, calc-silicate, amphibolite, and ultrabasic rocks (Paleoproterozoic); (3) paragneiss consisting metatexite and diatexite migmatite derived from greywacke sandstone, siltstone, and mudstone (Paleoproterozoic); (4) lower PIC units—migmatized and foliated hypersthene granite with diorite sheets and a layered structure imparted by sills of leucocratic garnet granite, hypersthene-quartz-feldspar granite, and flattened inclusions of paragneiss and diorite (Fig. 5G); (5) massive PIC units—homogeneous, massive hypersthene granite, feldspar-phyric with mineral magmatic state fabrics (Fig. 5H), likely comprising several unmapped intrusive units; and (6) leucocratic granite sills, dikes, and veins emplaced in paragneiss and in the lower PIC units.

At the base of the complex, the contact between paragneiss and the lower PIC unit is generally distinct (Fig. 4B). Both are diatexite migmatites (Rosa et al., 2018). The lower PIC units are generally massive and contain patches of coarse-grained hypersthene-quartz-feldspar leucosome within slightly more melanocratic biotite-hornblende-garnet-hypersthene-quartz-feldspar melanosome, whereas neosome in the paragneiss typically has diffuse layering (transposed bedding) in some cases with trails of peritectic garnet that mark relict bedding (Fig. 4G). Both neosomes have been deformed and have a moderate- to strong-intensity, composite crystal-plastic planar fabric ($S_1 + S_2 \pm S_3$). The crystal-plastic shape fabric in the lower PIC is defined by hypersthene, feldspar, and quartz and is parallel to the base of the complex. A linear fabric element is hard to find, although some steeply dipping joint surfaces in the dip direction show consistent top-to-the-W to top-to-the-NW asymmetric porphyroclast systems (Fig. 5F). Away from the contact, and higher in the complex, the crystal-plastic fabric intensity decreases and euhedral potassium feldspars with recrystallized rims define a modified magmatic state fabric (Fig. 5H). Both planar fabric elements are parallel to the base of the complex. Near the base of the complex, the lower PIC unit has been interleaved with paragneiss at large (100–500 m) and small scale, due either to primary igneous sheeting at the contact (an intrusive relationship) or to later thrusting and/or folding (a tectonic relationship) (Fig. 3) (Sleath, 2021).

On Lange Ø (Akia), a Ramsay type 2 (mushroom-crescent-dome) F_2-F_3 fold interference pattern in the base of the PIC and the underlying paragneiss has been refolded by N-S–trending, west-overturned F_4 folds (Fig. 3). In the paragneiss, planar fabrics ($S_0 + S_1$) were transposed to S_2 ($S_0 + S_1 \rightarrow S_2$) in F_2 fold limbs and folded again by F_3. The intensity of the composite fabric ($S_0 + S_1 + S_2 + S_3$) increases structurally upward into the shear zone at the base PIC (Sleath, 2021). The F_4 folds have a weak- to moderate-intensity, quartz-feldspar shape fabric in the axial plane (S_4). These close to tight folds (F_4) comprise a prominent N-S–trending belt of large-scale folding and fabric formation that crops out along the coast between Upernavik and Proven (Kangersuatsiaq) (Fig. 3). They refold at least one earlier phase of isoclinal folds, but the F_2-F_3 superposed fold pattern, although likely present, has been mapped only where there is good lithostratigraphic control, as at Lange Ø.

East of this belt of close to tight D_4 folding, large-wavelength, upright to NW-inclined, highly non-cylindrical D_4 folds deform the base of the PIC and have an envelope that dips very gently SE (Figs. 3 and 6C). Consequently, for ~60 km south and east of the northern margin of the complex, hypersthene granite of the lower and massive PIC units is exposed in large-scale synforms, and highly deformed diatexite paragneiss is exposed in large-scale antiforms, where erosion has provided windows into the migmatites below the floor of the complex. The largest of these are a dome-like antiform on Atilissuaq with steeply dipping limbs and a tube- or sheath-like shape, and a Ramsay type 2 (dome-crescent-mushroom) fold superposition pattern between east Nutaamiut and Nuna J.P. Koch (Fig. 3).

Internal Structure

The massive PIC unit is characterized by coarse-grained hypersthene granites with orthoclase feldspar and hypersthene phenocrysts aligned in magmatic state fabrics (Fig. 5H) with either very weak or no crystal-plastic fabrics. Variation in packing density of feldspar phenocrysts and mineralogical variation define lithological banding, which is parallel to the magmatic state fabric and the intrusion floor. Magmatic layering and magmatic state fabrics have been deformed by open, kilometer-scale upright to steeply inclined folds (Fig. 3). These trend E-W (F_3) and N-S (F_4), and superposition resulted in a Ramsay type 1 interference pattern (dome and basin) (Figs. 3, 6C, and 9).

South of Laksefjorden (Eqalugaarsuit Sulluat), the PIC is characterized by open to close, upright to steeply inclined, S-vergent folds (F_3) of the magmatic state planar fabric, and weak crystal-plastic fabrics. The folds trend E-W and have a wavelength of ~5 km (Figs. 3 and 8F). Toward the base of the complex, at Tasiusaq (Fig. 3), magmatic state fabrics were overprinted by N-dipping, crystal-plastic planar fabrics with recrystallization of orthoclase phenocrysts to form augen gneiss (Fig. 10A). The lower PIC unit crops out at the base of the complex and was intruded by garnet leucogranite sheets which dip N, parallel to a weak to moderate crystal-plastic foliation (Fig. 3) (T. Kokfelt, personal commun., 2023).

Southern Margin

Highly deformed, migmatitic meta–greywacke sandstones of the Nûkavsak Formation (paragneisses) dip gently to moderately steeply NW below the southern margin of the PIC (Figs. 3 and 10B) (Grocott and Pulvertaft, 1990). They are hypersthene-bearing, garnet-biotite metatexites and diatexites with strong fabric intensity—petrographically like those below the northern contact—and they, also, are host to a leucocratic granite sill, dike, and vein complex (Larsen and Grocott, 1991; Sleath, 2021; Guarnieri et al., 2022c). At Eqaluit, the complex is underlain by diatexite paragneisses with a paleosome of silicious resistor lithologies that dip N, parallel to the contact (Fig. 10C). The neosome has a leucosome of hypersthene granite and a melanosome of biotite (-hornblende)-pyroxene-quartz-feldspar. The neosome and paleosome were strongly deformed, and a quartz-feldspar crystal-plastic planar fabric is parallel to the resultant stromatic layering ($S_0 + S_1 \rightarrow S_2$). A fold hinge and/or intersection lineation is parallel to a WNW-plunging mineral stretching lineation ($L_1 \rightarrow L_2$) (Fig. 8F). The metamorphic field gradient decreases south and east, down-section from the PIC, and is marked by hypersthene and sillimanite + melt isograds (Fig. 3) (Grocott and Vissers, 1984; Grocott et al., 1987; Larsen and Grocott, 1991; Rosa et al., 2017, 2018). In the southern part of eastern Svartenhuk Halvø (Nunavik), metamorphic grade in the Karrat Group is at upper greenschist facies increasing to upper amphibolite facies, with anatexis, at the basement-cover contact (Fig. 3) (Grocott and Vissers, 1984).

South Rinkian FTB

On eastern Svartenhuk Halvø (Nunavik) and Inngia, two phases of deformation are recognized in metasedimentary rocks of the Karrat Group—Nûkavsak and Qaarsukassak Formations—and orthogneisses of the Archean basement (Fig. 3) (Grocott and Vissers, 1984; Grocott et al., 1987; Larsen and Grocott, 1991). The first is characterized by large- and small-scale, close to tight folds that plunge gently to moderately N with moderate to steep, W-dipping axial surfaces and vergence to the E (F_1) (Figs. 3 and 10D). The folds and related thrusts belong to an E-vergent thrust system—the Karrat Fjord thrust system—a regionally important early phase of thrusting in the south Rinkian FTB (D_1) (Grocott and McCaffrey, 2017; Guarnieri and Baker, 2022). The thrust system was reworked during a phase of thick-skinned inversion tectonics expressed as dome- and basin-like folds of the basement-cover contact and a system of W-vergent folds and thrusts (D_2) (Henderson, 1969; Grocott and McCaffrey, 2017) throughout the south Rinkian FTB, including the southern part of eastern Svartenhuk Halvø (Nunavik) (Fig. 3) (Grocott et al., 1987).

In south-to-north transects through glacial valleys at Umiarfik-Tasiusaq, Kangiusap Aaffaa, and Ukkusissat Sulluat, folds, thrusts, and fabrics of the Karrat Fjord thrust system become progressively transposed (overprinted) by D_2 ($S_0 + S_1 \rightarrow S_2$) ($L_1 \rightarrow L_2$) with transposition complete at a line more-or-less coinciding with the structurally lowest leucogranite intrusions in the sill complex underlying the PIC (Fig. 3) (Grocott and Vissers, 1984; Larsen and Grocott, 1991; Guarnieri et al., 2022c; T. Kokfelt, personal commun., 2023). In the high-temperature shear zone below the PIC, the main planar fabric is bedding transposed to a strong biotite planar fabric ($S_0 \rightarrow S_1$) folded by tight to isoclinal folds (F_2) with a new planar fabric (S_2) in the axial plane and transposition of the planar fabric to S_2 in fold limbs ($S_0 + S_1 \rightarrow S_2$) (Fig. 10E). Fold hinge lines plunge gently WNW-ESE, parallel to a biotite stretching lineation ($L_1 \rightarrow L_2$) (Fig. 8G). Leucocratic granite intrusions are folded isoclinally with S_2 in the axial plane and strong boudinage in the fold limbs (Fig. 10E). On the other hand, some intrusions are strongly discordant, particularly in the Ukkusigssat Sulluat transect, implying that they were emplaced post-S_2. Asymmetric quartz-vein boudins in paragneiss and in the underlying basement orthogneiss (Fig. 10F) show that the transport direction during D_2 was top-to-the-W, consistent with W vergence of asymmetric F_2 folds. The transposed planar fabric ($S_0 + S_1 + S_2$) and the granite sheets were deformed by open to tight, S-vergent, large-scale F_3 (Figs. 3 and 6C).

In summary, the evidence from the southern margin of the PIC shows that it has been thrust W or WNW by a major D_2 ductile shear zone. Thrusting was accompanied by anatexis and emplacement of leucocratic granite intrusions. East-vergent structures in the Karrat Fjord thrust system (D_1) were overprinted and transposed in this shear zone. Farther north, the D_2 shear zone is exposed in structural windows through the floor of the PIC and emerges at the northern margin of the complex, albeit overprinted by the Tussaaq shear zone—a zone of high D_4 deformation. The structure of the north Rinkian FTB has been described using deformation phases, D_1–D_5, based on overprinting relationships observed in the field. The kinematics of these deformation phases and proposed correlations across the PIC between the north and south Rinkian FTBs are summarized in Figure 9. It is unlikely that each of these phases represent a common deformation event at the same time at all localities.

TARGETED SAMPLES

U-Pb analysis was carried out on zircon separated from nine Karrat Group and three leucocratic granite samples (Fig. 11). Four samples, including three

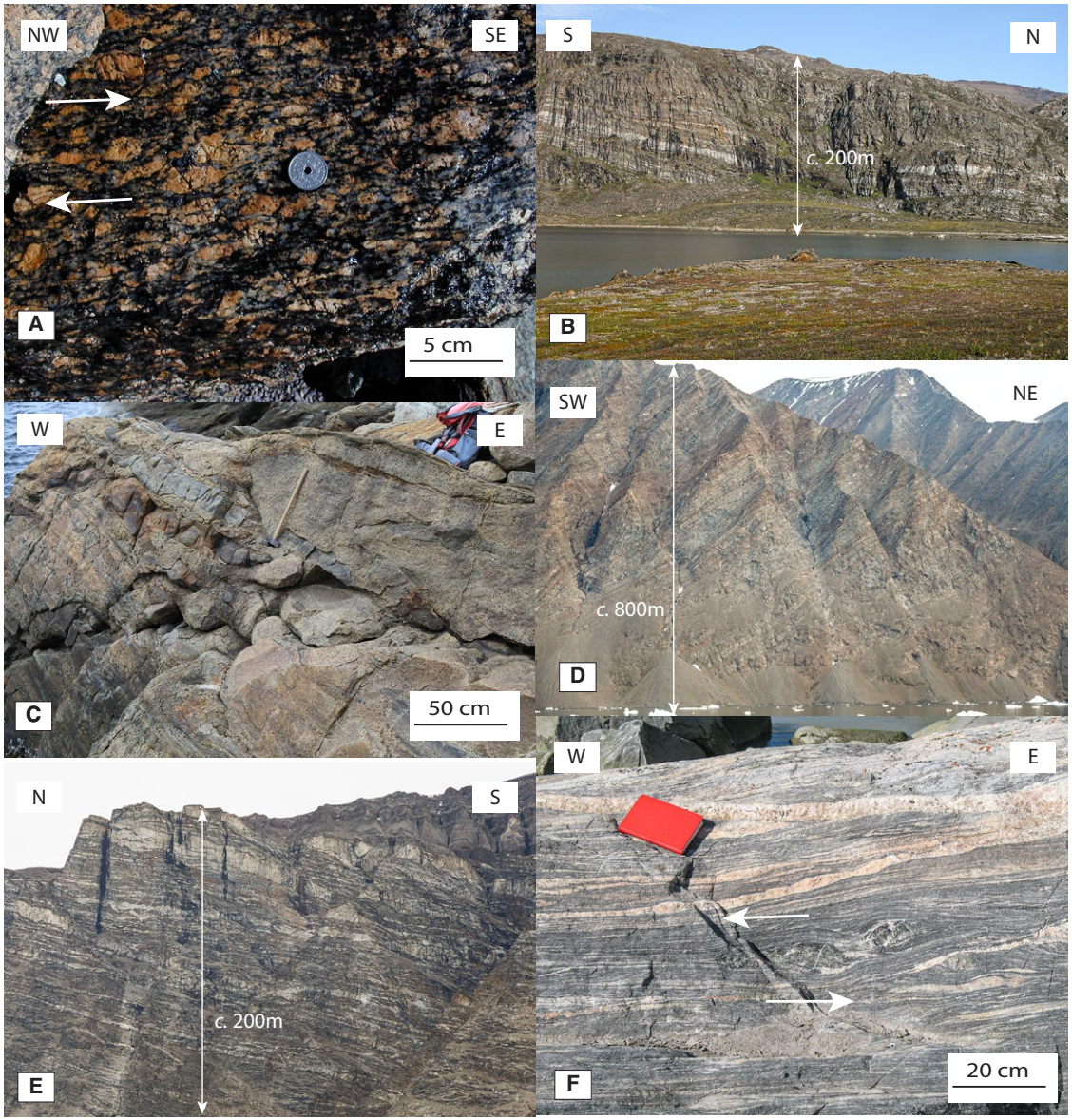

Figure 10. (A) Crystal-plastic deformation of magmatic orthoclase in the southern Prøven Igneous Complex (PIC), Tasiusaq (72°14.9′N, 54°23.9′W). Asymmetry of the recrystallized phenocrysts implies dextral displacement (top-to-the-E) during D_1 on a gently W-plunging stretching lineation (L_1). (B) N-dipping leucocratic granite sill complex in granulite facies metatexite paragneiss dipping N below the PIC, Tasiusaq (72°12.0′N, 54°29.2′W). (C) Granitic leucosome cutting N-dipping quartz arenite paleosome in paragneiss either just below the lower contact of the PIC or in a large inclusion in the PIC at Eqaluit (72°14.6′N, 54°54.9′W). (D) Close to tight, W-vergent folds (F_1) in Nûkavsak Formation, Karrat Fjord thrust system, eastern Nunavik (71°48.2′N, 53°28.8′W). (E) Strongly boudinaged and isoclinally folded leucocratic granite sills in paragneiss with bedding and S_1 transposed to a gently S-dipping differentiated layering (S_2) in the limb of an open F_3 fold, Ukkusissat Sulluat (72°09.1′N, 53°40.8′W). (F) High S_2 fabric intensity in orthogneiss, Pannertooq basement high (72°16.2′N, 53°44.8′W). Asymmetric boudins in the mafic horizon have sinistral asymmetry on a shallow W-plunging stretching fabric (L_2) consistent with top-to-the-W displacement.

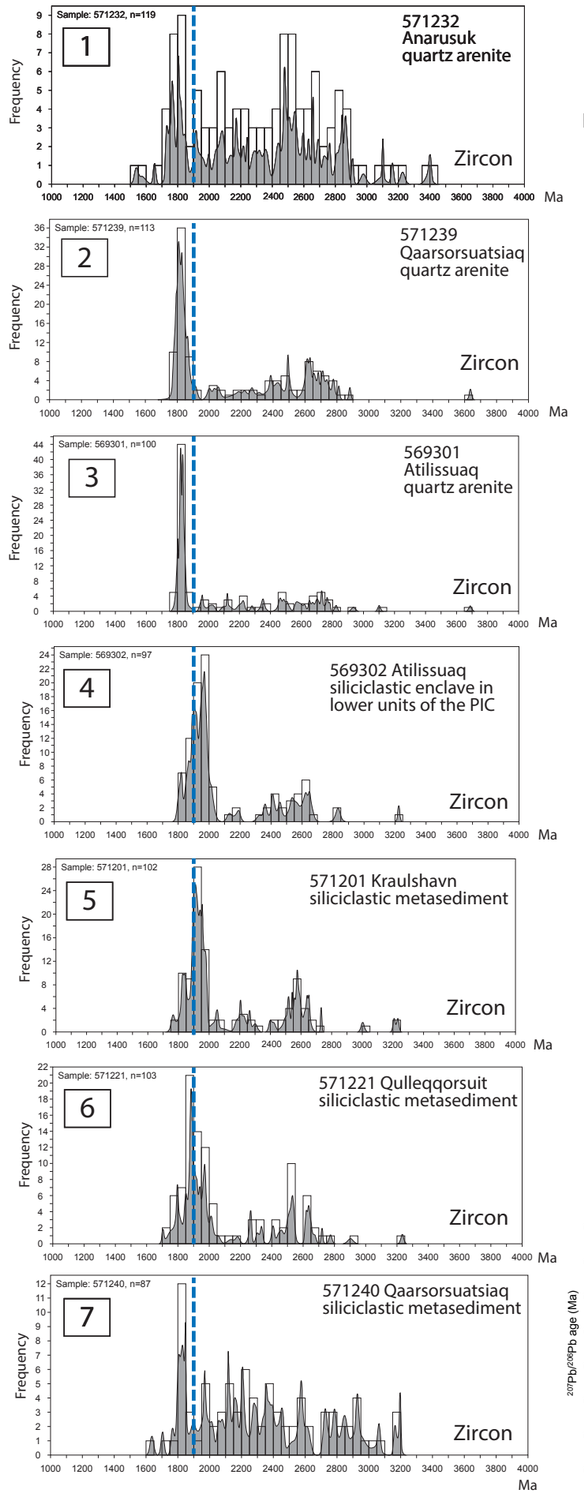

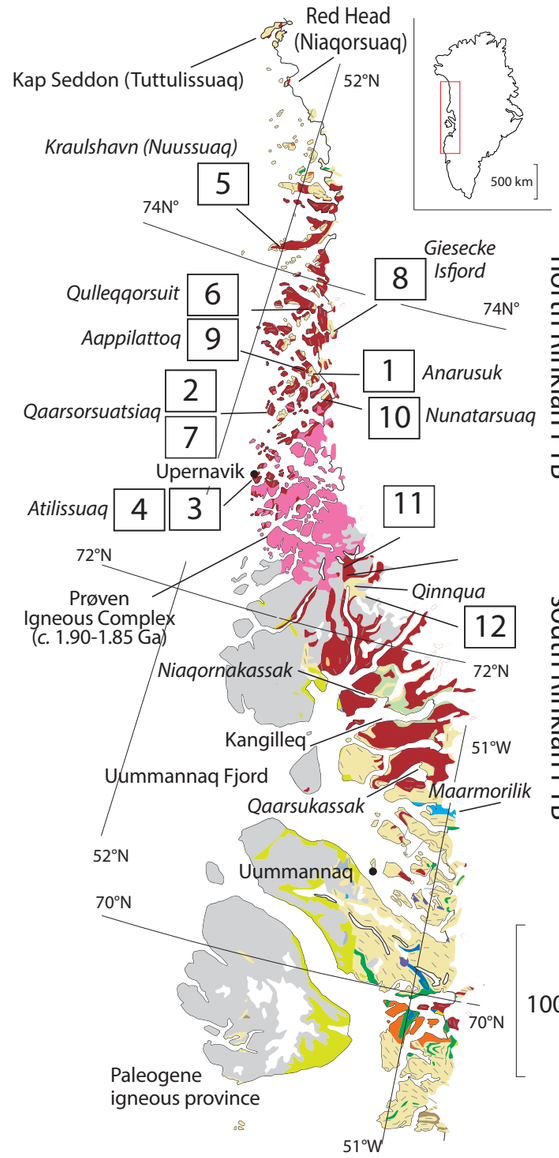

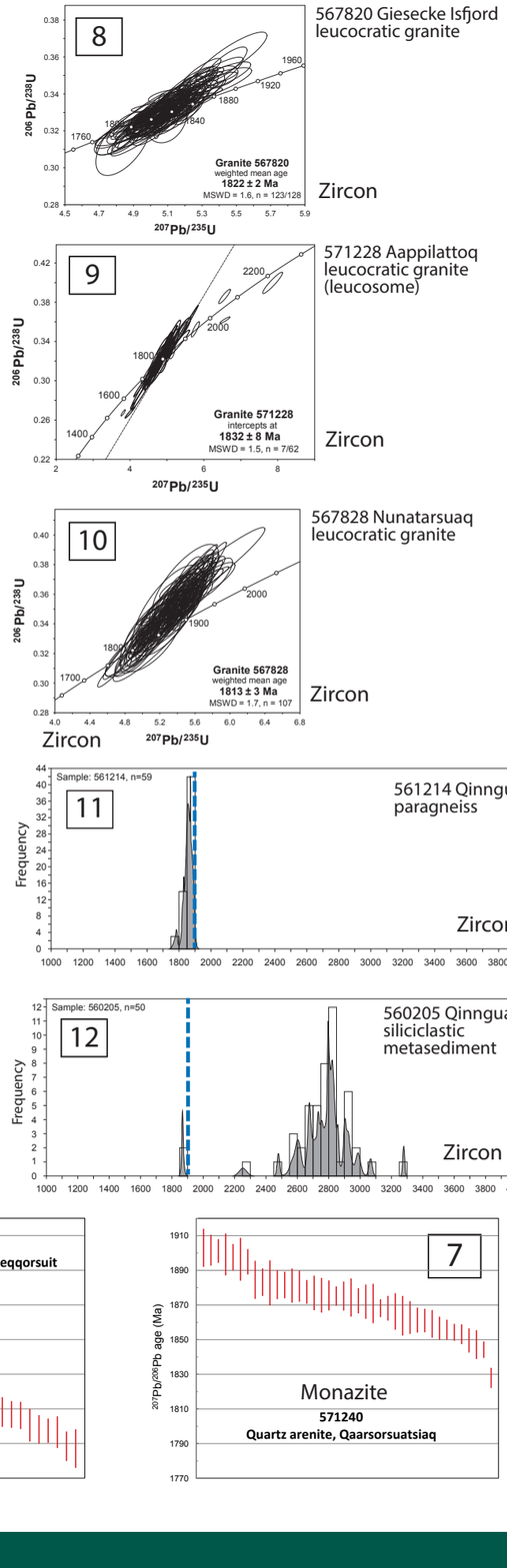

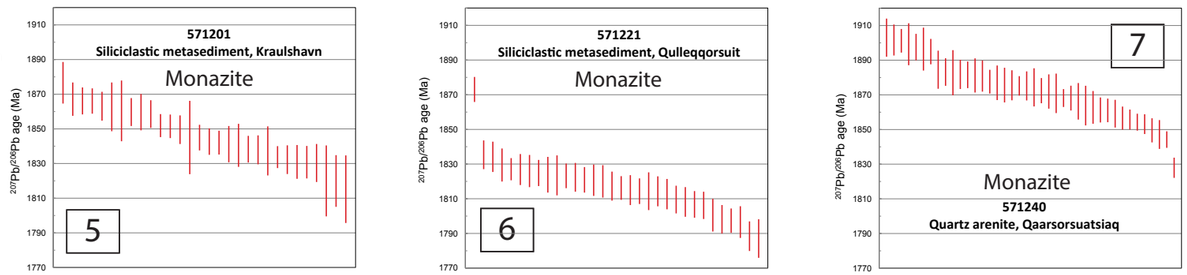

Figure 11. U-Pb age results. Map shows sample locations; see Figure 1A for geologic unit explanation. Histogram–probability density diagrams are shown for zircon results from nine samples from the Karrat Group. Monazite age distribution plots (in red) are shown for three of these samples from the Nûkavsak Formation in the north Rinkian fold-thrust belt (FTB). Monazite plots show that there was a continuous metamorphic overprint from ca. 1900 Ma to 1800 Ma, not just one short event. U-Pb concordia diagrams are shown for three samples of leucocratic granite. Blue vertical dashed line at 1900 Ma in the histogram–probability density plots indicates the emplacement of the earliest intrusions in the Prøven Igneous Complex (PIC) and the oldest (metamorphic) monazites. It is therefore our best estimate of the onset of high-temperature metamorphism.

selected for monazite analysis, were siliciclastic rocks from the Nûkavsak Formation (samples 561214, 571201, 571221, 571240) and one was a metasandstone inclusion from the lower PIC (569302). Three samples were meta–quartz arenite (569301, 571232, 571239) and one sample a garnet-mica schist (560205), all from the Qaarsukassak Formation. These samples were collected to constrain: (1) the age range of detrital zircon and hence of the magmatic arcs eroded to supply sediment to the Karrat Group basin; (2) the maximum deposition age of detrital zircon; and (3) the age of metamorphic zircon grains and overgrowths and of metamorphic monazite grains, to determine the age and duration of metamorphism in a well-constrained structural framework (D_1–D_5). Three leucocratic granite samples were collected to constrain ages of: (1) a syn-tectonic leucocratic granite (567820); (2) a diatexite migmatite (peak metamorphism) (571228); and (3) a late- to post-tectonic leucocratic granite (567828).

Analytical Methods (File S2)

Rock samples were prepared for analysis at GEUS. Zircon analysis at GEUS was by laser ablation inductively coupled plasma mass spectrometry (LA-ICPMS) using a Thermo-Scientific ELEMENT2 sector field inductively coupled plasma mass spectrometer (SF-ICPMS) coupled to a NWR UP213 laser ablation unit equipped with a frequency-quintupled, solid-state Nd:YAG laser. Monazite analysis was by secondary ion mass spectrometry (SIMS) using the Cameca IMS1280 large-format high mass resolution ion microprobe at the Swedish Museum of Natural History, NordSIM facility. The analytical methods used are described in detail in File S2.

RESULTS FROM GEOCHRONOLOGY

Histogram–probability density diagrams show the age distribution of detrital and metamorphic zircons from metasedimentary rocks, and concordia diagrams give the crystallization age of leucocratic granite samples (Fig. 11; Tables S1 and S2 [see footnote 1]). The collection localities are identified by a reference number used in the descriptions that follow (1, 2, 3 etc.; Fig. 11).

Karrat Group, North Rinkian FTB

Quartz Arenite, Anarusuk (Sample 571232) (1)

Sample 571232 was collected from an ~150-m-thick sequence of meta–quartz arenite, marble, and amphibolite folded with migmatized mica schist in a F_2-F_3 interference pattern. Zircon grains are dominantly stubby and rounded, most have zoned cores with distinct overgrowths, and many are cracked (Fig. 12A). One hundred nineteen (119) analyses yield a continuous $^{207}Pb/^{206}Pb$ age range from 3402 ± 15 Ma to ca. 1500 Ma, with two large peaks in the range 2500–2450 Ma and 1850–1800 Ma, though neither is dominant. $^{207}Pb/^{206}Pb$ ages younger than 1900 Ma generally have Th/U ratios <0.1, whereas grain cores older than 1950 Ma have Th/U ratios >0.1 (Table S1). Grains with ages between 1950 and 1900 Ma have large uncertainties and low Th/U ratios (Table S1).

Quartz Arenite, Qaarsorsuatsiaq (Sample 571239) (2)

Sample 571239 is from an ~100-m-thick sequence of meta–quartz arenite, schist, and mafic rocks underlying the Nûkavsak Formation (sample 571240). The mafic rocks have a granulite facies assemblage of orthopyroxene, clinopyroxene, plagioclase, and minor hornblende. Folds (F_2) in the basement-cover contact nearby have been refolded by F_3 and (likely) tightened during D_4. Unusually, bedding has not been transposed to the regional planar fabric. Zircon varies in size and shape; most grains are zoned, and many have broad rims (Fig. 12B) which are U rich relative to cores (Table S1). One hundred thirteen (113) analyses reveal a large and broad peak at ca. 1900–1750 Ma dominated by 1830–1800 Ma ages. Many are from grain peripheries and have Th/U ratios of ~0.1 (Table S1). There is a continuous range of Mesoarchean to Paleoproterozoic ages between 2882 ± 13 Ma and 2000 ± 8 Ma from zoned zircon grains. A single grain had an Eoarchean age of 3637 ± 15 Ma.

Quartz Arenite, Atilissuaq (Sample 569301) (3)

The upper part of a quartz-arenite sequence was sampled immediately below the lower PIC unit in the hinge zone of the Atilissuaq anticline (sample 569301). Zircon varies from small and round or stubby to large and more elongated (75–250 µm maximum dimension). Most have irregular patterns, and many have wide rims, though some still preserve original zonation (Fig. 12E). One hundred (100) grains were analyzed. Ages range from 3689 Ma to 1784 Ma dominated by a very large peak at ca. 1850–1800 Ma with a few ages both older and younger. Ages from the peak are from rims and grains with irregular patterns, and their Th/U ratios are generally lower than for the older zircons although most ratios are >0.1 (Table S1).

Siliciclastic Inclusion, Lower PIC, Atilissuaq (Sample 569302) (4)

Medium-grained, recrystallized biotite-quartz metasediment from a slightly flattened, *c.* 20cm diameter inclusion in foliated diatexite was collected from the lower PIC (sample 569302), just above the Nûkavsak Formation. Zircon grains range from 75 µm to 150 µm in maximum dimension and are stubby to elongate with round edges. Zonation varies from oscillatory to complex-diffuse (Fig. 12C). Results from 97 zircons are dominated by a large, broad peak at ca. 2050–1800 Ma with the mode between ca. 2000 Ma and 1950 Ma.

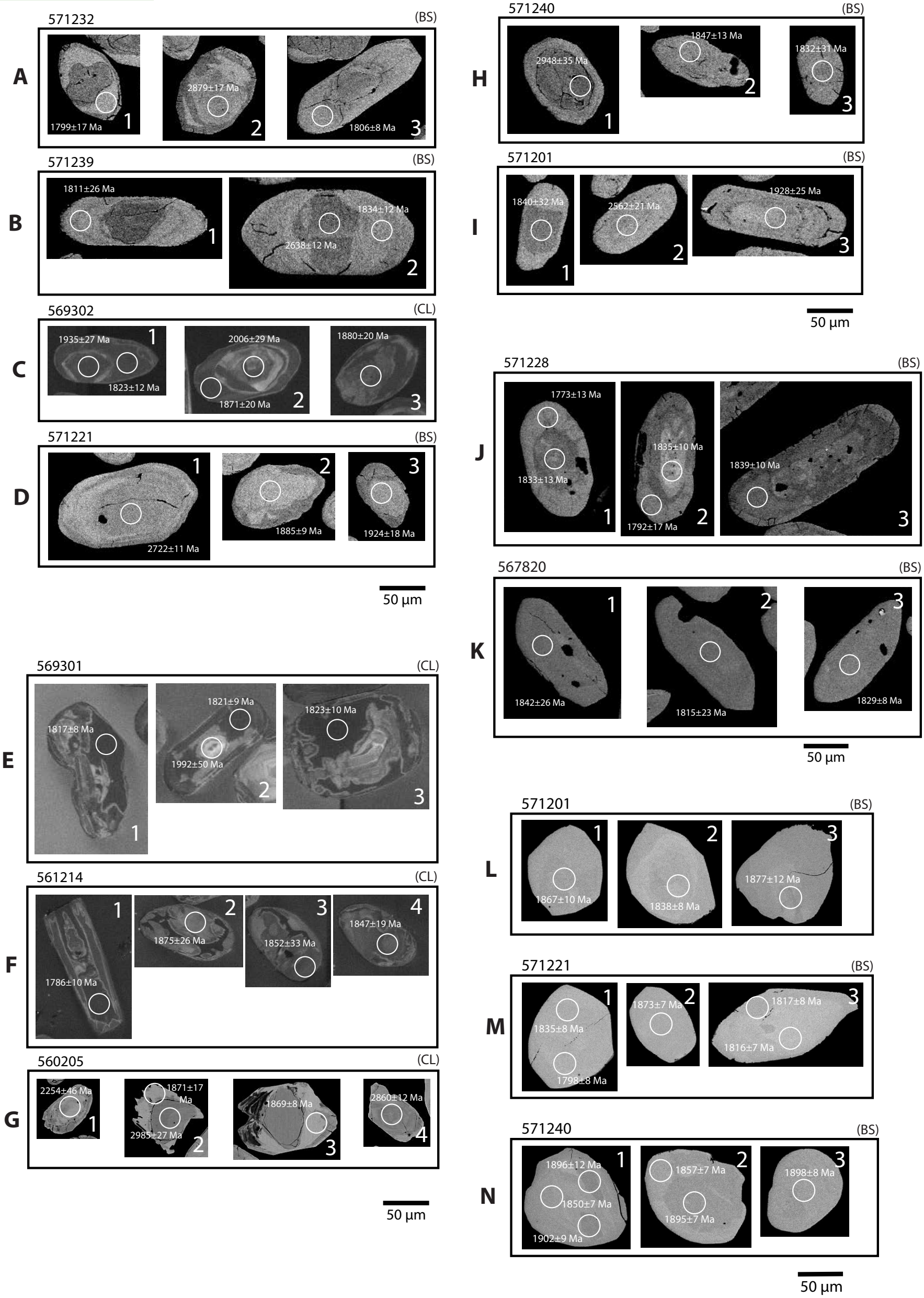

Figure 12. Microstructures of analyzed zircon (A–K) and monazite (L–N). Circles show the location of analytical pits: 30 µm for zircon, 20 µm for monazite. BS indicates back-scattered electron microscope images, and CL indicates cathodoluminescence images.

In addition, there are some Archean ages, and this distribution is typical for the Nûkavsak Formation (Sanborn-Barrie et al., 2017). The ages at ca. 1900–1800 Ma are from grain peripheries or from grain cores with complex-diffuse microstructure (Fig. 12C). There is a subsidiary peak from grain rims at ca. 1820 Ma.

Siliciclastic Metasediment, Kraulshavn (Nuussuaq) (Sample 571201) (5)

A sample of brown-weathered metatexite (sample 571201) was collected near the base of the Karrat Group in the limb of a D_2 syncline. One hundred two (102) zircon grains were analyzed. They are small, gray, and stubby to elongate with round edges (Fig. 12I). $^{207}Pb/^{206}Pb$ ages range from 3233 Ma to 1765 Ma dominated by a peak at ca. 2000–1900 Ma. Monazite grains in this sample range from 50 µm to 100 µm in size. They are clear, sub-rounded, and mostly homogeneous, though a few show vague zonation (Fig. 12L). Thirty (30) spots were analyzed. The results are concordant but do not yield a single age. Rather, they yield a continuum of ages from ca. 1875 Ma to 1810 Ma.

Siliciclastic Metasediment, Qulleqqorsuit (Sample 571221) (6)

A sample of brown-weathered, garnet-rich metatexite (sample 571221) was collected from the Nûkavsak Formation on Qulleqqorsuit near the base of the Karrat Group in the lower limb of a W-vergent D_3 fold, just below the leucocratic granite sill complex. One hundred three (103) zircon grains were analyzed. They are clear to gray-brown and range from stubby to elongate with rounded edges. Some have zonation (Fig. 12D). A single grain had a $^{207}Pb/^{206}Pb$ age of 3235 Ma. The rest have ages ranging from 2905 Ma to 1797 Ma, with the majority in the range ca. 2000–1800 Ma and the mode at ca. 1885 Ma. Monazite grains are pale yellow, clear, sub-rounded, and mostly homogeneous; a few show vague zonation (Fig. 12M). Thirty-two (32) spots were analyzed, several from monazites with zonation that yielded the same age in various domains. It was not possible to obtain a single age from all the analyses. Instead, the results yield a continuum from ca. 1840 Ma to 1790 Ma, with a single grain at ca. 1875 Ma.

Siliciclastic Metasediment, Qaarsorsuatsiaq (Sample 571240) (7)

A sample of metasiltstone (sample 571240) was collected from a sequence of meta–volcaniclastic (epiclastic) sandstone and siltstone in the Nûkavsak Formation. The siltstone was interbedded with garnet-cordierite-sillimanite schist and overlies quartz arenite (sample 571239), schist, and mafic horizons in an F_2-F_3 superposed fold pattern, likely tightened during D_4, at the northern margin of the Tussaaq shear zone. Eighty-seven (87) zircons were analyzed. The population is dominated by stubby to rounded grains that are small and brownish (Fig. 12H). Some show zonation, with many having fractures and others being partly resorbed (Fig. 12H). The $^{207}Pb/^{206}Pb$ age range is from 3198 Ma to 1638 Ma, a pattern not distinctly different from that of the underlying quartz arenite (sample 571239), except that the peak, here dominated by ca. 1850–1810 Ma ages, is smaller. Monazites from this sample (n = 40) are pale yellow, clear, round, and homogeneous (Fig. 12N) and yielded a continuum in a range from ca. 1900 Ma to 1830 Ma.

Leucocratic Granite, North Rinkian FTB

Leucocratic Granite, North of Giesecke Isfjord (Kangerlussuaq) (Sample 567820) (8)

Sample 567820 was collected from an ~500-m-thick sill of medium- to coarse-grained, biotite-hornblende granite emplaced into metatexite metasediment (Fig. 4C), parallel to transposed bedding in metasediment screens between intrusions ($S_0 + S_1 + S_2 + S_3$). Narrow sills nearby are strongly boudinaged in S_2-S_3, although the main sheet is concordant and has not been boudinaged. Large dikes of granite cut across the fabric in the metasediment screens. The granite is therefore syn- to late tectonic—probably late D_2-D_3. The zircon grains are stubby to elongated and mostly round with many inclusions. A few show zonation (Fig. 12K). One hundred twenty-eight (128) grains were analyzed, and 123 yield a weighted mean $^{207}Pb/^{206}Pb$ upper intercept age of 1822 ± 2 Ma (mean square of weighted deviates [MSWD] = 1.6).

Leucocratic Granite (Leucosome), Aappilattoq (Sample 571228) (9)

Granitic leucosome (sample 571228) was collected from Archean gneiss interleaved with Nûkavsak Formation during D_1 and folded by an F_2 isocline in a F_2-F_3 fold superposition pattern. Sixty-two (62) spots were analyzed. Many zircon grains have magmatic zoning and others a diffuse zoning (Fig. 12J). Ages range from 2250 Ma to 1700 Ma, with the main cluster between ca. 1850 Ma and 1700 Ma. The seven oldest grains from the cluster yield an age of 1832 ± 8 Ma (MSWD = 1.5). All except the oldest grain have Th/U <0.1 (Table S1).

Leucocratic Granite, Northwestern Nunatarsuaq (Sample 567828) (10)

Sample 567828, from a weakly foliated, biotite-hornblende granite dike, was collected in the Tussaaq shear zone. The dike is discordant and cuts sharply across transposed bedding in paragneiss ($S_0 + S_1 + S_2 + S_3 + S_4$) and a folded hypersthene granite sheet of the PIC. It was emplaced late- to post-D_4. Zircons are mostly stubby with well-preserved magmatic zonation. One hundred seven (107) analyses yield a weighted mean $^{207}Pb/^{206}Pb$ age of 1813 ± 3 Ma (MSWD = 1.7).

Karrat Group, South Rinkian FTB

Paragneiss, North of Qinngua Basement High (Sample 561214) (11)

A medium- to coarse-grained granulite facies paragneiss with orthopyroxene and biotite (sample 561214) was collected ~1 km below the PIC. The paragneiss is shown as Nûkavsak Formation on published maps. Bedding has been transposed to a planar crystal-plastic fabric ($S_0 + S_1 + S_2$). The zircons are 75–150 µm in size and round to elongated. The zonation pattern in most grains is highly irregular and disturbed (Fig. 12F) and many have high-U domains. Fifty-nine (59) analyses give ages from ca. 1900 Ma to ca. 1775 Ma, with the mode at ca. 1870 Ma and two smaller peaks at ca. 1830 Ma and ca. 1785 Ma. Th/U ratios range from 0.81 to 0.06 (Table S1).

Siliciclastic Metasediment, South of Qinngua Basement High (Sample 560205) (12)

Sample 560205 is an upper amphibolite facies, non-migmatitic, garnet-mica schist collected at the base of the Karrat Group. The schist is interbedded with psammite, and bedding has been transposed to a planar fabric parallel to the basement-cover contact ($S_0 + S_1 + S_2$) and differentiated layering within underlying Archean gneiss ($S_1 + S_2$). Decimeter- to meter-scale dike and vein systems of leucocratic granite cut sharply across this fabric in metasedimentary rock and in basement. Zircons are small, the majority <100 µm in length. Some have oscillatory zoning, and most have irregular rims (Fig. 12G). Fifty (50) ages range from ca. 3280 Ma to ca. 1870 Ma, with the vast majority being Archean. Only two ages, both from rims with low Th/U ratios, are younger than 1900 Ma, defining a small peak at ca. 1870 Ma (Fig. 12G, images 2–3).

DISCUSSION

Significance of the U-Pb Results

Quartz Arenites (Samples 571232, 571239, 569301), North Rinkian FTB

In the quartz arenite samples (569301, 571232, 571239), zircon grains yielding U-Pb ages >1950 Ma typically have Th/U ratios >0.1 and are interpreted as detrital grains. Grains with unambiguous detrital igneous characteristics were used to determine youngest detrital zircon (YDZ) ages of 2000 ± 8 Ma (sample 571239) and 1949 ± 16 Ma (569301). Large uncertainties are associated with ages in the 1950–1900 Ma range, and although grain cores and rims are mainly characterized by low Th/U ratios, microstructural criteria did not allow a consistent distinction between detrital and metamorphic grains. We are unable to prove a maximum deposition age for the lower Karrat Group (Qaarsukassak Formation) younger than ca. 1950 Ma.

Analyses from high-uranium rims and other domains yield ages <1900 Ma and define a prominent peak at ca. 1850–1800 Ma. Low Th/U ratios (<0.1) imply that these are volumes of the grains that have been recrystallized (metamorphic). Close to the PIC, however, Th/U is >0.1 for most analyses in this age range, although still generally lower than for the older grains (sample 569301). Nevertheless, heterogeneous patchy patterns and convolute zoning show that the grains have been heavily affected by metamorphism and evidence of magmatic zonation has been mostly destroyed (Fig. 12E). We interpret the relatively high Th/U ratios as due to open-system metamorphism close to the complex (Yakymchuk et al., 2018) and these grains as metamorphic. The peak at ca. 1850–1800 Ma spans the crystallization age of leucogranites and granitic leucosomes (samples 567820, 571228, 567828). It is interpreted to give the age of high-temperature metamorphism.

Siliciclastic Metasediments, North Rinkian FTB (Samples 571201, 571221, 571240, 569302)

The U-Pb results from samples 571201, 571221, 571240, and 569302 are dominated by large, broad peaks at ca. 2050–1800 Ma with the mode varying between ca. 2000 Ma and 1900 Ma. In sample 571240, a positive skew in the data is less obvious, and the mode is instead at 1830–1800 Ma. Our microstructural observations do not allow a distinction between detrital and metamorphic grains to be made, and, somewhat paradoxically, Th/U ratios are generally higher for the younger zircons in this group—possibly reflecting open-system melting during high-grade metamorphism—but nevertheless again leaving ambiguity in the distinction between metamorphic and detrital grains and difficulty in identifying the YDZ. More straightforwardly, amorphous metamorphic grain cores and rims yield subsidiary (571201, 571221) to dominant (571240) peaks at ca. 1850–1800 Ma, consistent with the age range for high-grade metamorphism of the quartz arenite samples. Monazite grains yielded ages between ca. 1900 Ma and 1800 Ma, interpreted as a continuous metamorphic overprint during this time interval. The monazite ages, in combination with the intrusion ages of the PIC and the leucogranites, imply that all the zircon grains younger than ca. 1900 Ma are metamorphic.

In the metasedimentary inclusion from the lower PIC unit (sample 569302), complex-diffuse zonation in zircon grain cores and wide, dark-gray rims, both with ages of ca 1900–1800 Ma, are interpreted as due to recrystallization of detrital grains (Fig. 12C). Although some zoned cores may well be detrital igneous in origin, many irrefutably metamorphic domains have Th/U ratios of 0.25–0.15. The probability-density plot implies that the inclusion was metamorphosed either: (1) at ca. 1900 Ma and again during a separate ca. 1820 Ma event or (2) during a single, prolonged, metamorphic event ca. 1900–1800 Ma.

Siliciclastic Metasediments, South Rinkian FTB (Samples 561214, 560205)

The results of the U-Pb age data from sample 561214 are unique in that they yield a rather narrow age range from ca. 1900 Ma to ca. 1775 Ma. Zircon

grains show irregular and complex microstructures, and the magmatic zonation is mostly destroyed (Fig. 12F). All the grains are interpreted as recrystallized due to metamorphism at ca. 1900 Ma, notwithstanding Th/U ratios >0.1, which we ascribe to open-system behavior during recrystallization. In lower-grade garnet-mica schist from the Qaarsukassak Formation (560205), zircon grains with oscillatory zoning allow a YDZ to be identified at ca. 2250 Ma (File S3 [see footnote 1]). Two ages from overgrowths signal a metamorphic overprint at ca. 1870 Ma.

Sediment Provenance

Quartz Arenites (Qaarsukassak Formation)

Zircon age data from detrital grains in the quartz arenite–dominated lower part of the Karrat Group show a wide range of Paleo- Meso- and Neoarchean as well as Paleoproterozoic ages (Fig. 11) (samples 571232, 571239, 569301). The most likely source is the underlying Archean basement, which includes: (1) a ca. 2710 Ma orthogneiss at Holm Ø (Kiatassuaq) (Nutman et al., 2008); (2) a 2713 ± 6 Ma weakly foliated granite intruding Archean gneiss on nearby Amdrup Ø (Kiataasap); (3) orthogneiss from Inussulik Bugt (Inussullip Imaa) with upper intercept ages of 2644 ± 13 Ma and 2736 ± 7 Ma; and (4) farther south, at Paarnivik, a banded orthogneiss with several generations of leucosomes that have an age of 3168 ± 12 Ma, with evidence of younger components from clusters of ages at 3000–2900 Ma and 2700–2600 Ma (Thrane, 2021). Late Neoarchean grains and very early Paleoproterozoic grains also occur in the quartz arenite samples, but igneous rocks of these ages are rare in North and West Greenland and in Laurentia. They do crop out in the Thule complex of North Greenland (Nutman et al., 2008), implying—like the younger Paleoproterozoic peaks—that although the bulk of detrital grains in these samples could have been derived locally, some were derived from Neoarchean and earliest Paleoproterozoic magmatic arc sources distal to the Rinkian paleo–continental margin (Sanborn-Barrie et al., 2017).

The maximum depositional age of the quartz arenites is constrained by YDZ ages of 1949 ± 16 Ma (sample 569301) and 2000 ± 8 Ma (571239). This establishes a mid-Paleoproterozoic maximum depositional age for the lower Karrat Group in the north Rinkian FTB. The quartz arenites are associated with other lithostratigraphic units, including minor carbonate rocks, prompting correlation with the Qaarsukassak Formation (T. Kokfelt, personal commun., 2023). There are, however, differences between the lower Karrat Group quartz arenite units north and south of the PIC: (1) the detrital zircon age distribution in the Qaarsukassak Formation south of the PIC is dominated by Archean grains (560205)—Paleoproterozoic grains are few—whereas in the north, the age distribution points to a continuum of Archean and Paleoproterozoic ages without dominating peaks (571232); (2) metasedimentary rocks in the lower part of the Karrat Group in the north and south have different Archean-age detrital zircon distributions (Sanborn-Barrie et al., 2017; Thrane, 2021); and (3) quartz arenites north of the PIC have a distinctly younger maximum depositional age than the Qaarsukassak Formation to the south (ca. 1950 Ma [569302] and ca.2250 Ma [560205], respectively). The earliest Paleoproterozoic sedimentary subbasins, now separated by the PIC, had different sources of Archean-age detrital zircon, and in the north, there was an abundant source of ca. 2.5–2.0 Ga detrital zircon represented by only a few grains in samples collected to the south (560205). The Karrat Group subbasin in which the quartz arenite unit was deposited in the north Rinkian FTB may have been more proximal to eroding Neoarchean and earliest Paleoproterozoic magmatic arc rocks than the lower Karrat Group subbasin in the south Rinkian FTB, and it may have had a different history of structural inversion.

Siliciclastic Metasedimentary Rocks (Nûkavsak Formation)

According to Sanborn-Barrie et al. (2017), a "typical" detrital zircon age distribution for siliciclastic metasedimentary rocks of the Nûkavsak Formation is a spread of Meso- and Neoarchean grains and a few earliest Paleoproterozoic grains, but the hallmark is a large Paleoproterozoic detrital peak at ca. 2050–1950 Ma. While ca. 2050 Ma to 1950 Ma detrital ages are present in our Nûkavsak Formation data (samples 571201, 571221), they are overshadowed by large peaks at 1950 Ma to 1900 Ma from questionable detrital and/or in situ metamorphic grains. The monazite data from the Nûkavsak Formation (571201, 571221, 571240) indicate, however, that regional metamorphism did not commence before 1900 Ma—about the time that the first intrusions of the PIC were emplaced. Therefore, although microstructural observations are not conclusive, most of the zircon grains in this age range are likely detrital. At Kraulshavn (Nuussuaq) (571201), the prominent peak at ca. 1913 Ma may well be from detrital grains and compares well with the 1905 ± 20 Ma YDZ age determined at Holm Ø (Kiatassuaq) (Fig. 3) (Sanborn-Barrie et al., 2017). The implication is that basin inversion, emplacement of the earliest intrusions in the PIC, and the onset of metamorphism all took place—probably in that order—at ca. 1900 Ma.

Metasedimentary Inclusions in the Lower PIC Unit

Metasedimentary inclusions are ubiquitous in the lower PIC, and a siliciclastic inclusion (sample 569302) was found to have a distribution of detrital zircon age ranges typical for the Nûkavsak Formation. Ages from the inclusion shed light on the maximum depositional age of the Nûkavsak Formation because an inclusion cannot contain a detrital grain that is younger than the intrusion that contains it. The lower PIC on Atilissuaq has an age of 1869 ± 9 Ma (Thrane et al., 2005). A few kilometers along strike, on Karrat, another unit in the lower PIC has an age of 1900 ± 4 Ma (Sanborn-Barrie et al., 2017). In our inclusion sample, grains and grain rims with ages in the intervals 1900–1850 Ma and 1850–1800 Ma are, therefore, certainly in situ metamorphic zircon grains. In

the interval 1950–1900 Ma, grains with a distinct peak at ca. 1908 Ma could be considered to be metamorphic—on this criterion—in which case the Nûkavsak Formation basin, at least close to the PIC, was inverted earlier and the PIC was emplaced into rocks that were already metamorphosed. More likely, these are detrital grains and the basin was still receiving sediment at, or later than, ca. 1908 Ma, just before intrusion of the early PIC units and prior to the start of regional metamorphism (D_1) at 1900–1875 Ma.

A minor peak at 1822 Ma points to continued metamorphism of the inclusion within the ca. 1875–1810 Ma age range that we assign to high-temperature deformation in and around the PIC during D_2-D_3-D_4. This is consistent with Sm-Nd and Lu-Hf isotope analysis on unleached garnet fractions from diatexite migmatite collected from the lower PIC units nearby, which yielded isochron ages of 1821 ± 18 Ma and 1820 ± 9 Ma, respectively (Thrane et al., 2005).

Age of Deformation and Metamorphism—North Rinkian FTB

The Nûkavsak Formation at Kraulshavn (Fig. 3) is a metatexite migmatite metamorphosed at high grade during D_1-D_2-D_3 in a structural domain characterized by F_2-F_3 fold superposition but relatively low D_3 fabric intensity. Zircon data have a broad peak at ca. 2000 Ma to 1800 Ma (sample 571201), with a prominent mode from grains slightly older than 1900 Ma in the 1950–1900 Ma interval that may be in situ metamorphic or detrital (Fig. 11). The oldest monazite found in this sample had an age of ca. 1875 Ma, and the monazite data in general imply onset of high-grade metamorphism and deformation (D_1) in the range of ca. 1900 Ma to ca. 1875 Ma. The sample from Qulleqqorsuit (571221), farther south, was collected at a higher structural level in a domain dominated by F_2-F_3 superposition, just below the leucogranite sill complex. The F_3 folds are tighter than at Kraulshavn, and F_2-F_3 have been reorientated during D_5 (Fig. 3). The broad peak of data at ca. 2000–1800 Ma is like that at Kraulshavn, and the mode at ca. 1885 Ma in the 1900–1850 Ma interval is interpreted to give an age for the onset of deformation (D_1) and high-grade metamorphism. Smaller peaks in the interval 1850–1800 Ma imply that recrystallization continued at both localities during later events (D_2-D_3-D_4-D_5).

South and east of a line between Tasiusaq Bugt and Ussing Brær (Fig. 3), and to higher structural levels than are exposed farther north, modal values in the age distribution from metamorphic zircon grains and rims shift from the 1950–1900 Ma and 1900–1850 Ma intervals to younger ages (Fig. 11) accompanied by increase in fabric intensity, metamorphic grade, and anatexis together with emplacement of a leucocratic granite sill complex. Quartz arenites (samples 571232, 571239, 569301) and the siliciclastic metasediment from Qaarsorsuatsiaq (571240) each have a modal value in the 1850–1800 Ma interval from metamorphic grains and rims. The age of an in-source leucosome in basement orthogneiss at Aappilattoq (Fig. 3) (571228) implies that high-temperature metamorphism and extensive partial melting of the siliciclastic metasedimentary sequence were happening at 1832 ± 8 Ma, probably during D_2. The 1813 ± 3 Ma age of a post-D_4, discordant leucocratic granite intrusion in the Tussaaq shear zone (567828) shows that extensive partial melting had ended by ca. 1810 Ma. Lower-temperature porphyroclastic textures present locally in the Tussaaq shear zone imply reactivation after this time.

This shift in data modes from the 1950–1900 Ma and 1900–1850 Ma intervals (samples 571201—Kraulshavn and 571221—Qulleqqorsuit) to the 1850–1800 Ma interval (571239 and 571240—Qaarsorsuatsiaq, 571232—Anarusuk, and 569301—Atilissuaq) could mean that deformation and metamorphism (D_1-D_2-D_3-D_4) are diachronous and become progressively younger to the south. However, there are widespread, though few, older ages from zircon grains and rims and monazite grains present in the data south of Tasiussaq Bugt and Ussing Brær, and in particular, the prominent peak at ca. 1900 Ma of metamorphic zircon grains in the PIC inclusion (569302) and ages at ca. 1900 Ma from monazite (571240) mitigate against this interpretation. Instead, we infer that southeast of Tasiusaq Bugt, deformation and regional metamorphism started sometime between ca. 1900 Ma and ca. 1875 Ma during D_1 but continued for longer with increasing proportions of partial melting and metamorphic grade that reached granulite facies during D_2 at 1832 ± 8 Ma, the age of leucosome in hypersthene-bearing basement orthogneiss at Aappilattoq (571228). D_4—which largely post-dated extensive partial melting in the paragneisses and overprinted D_1-D_2-D_3 folds and fabrics—is bracketed by sample 567820 (pre-D_4 leucocratic granite) and sample 567828 (post-D_4 leucocratic granite) between 1822 ± 2 Ma and 1813 ± 3 Ma.

Age of Deformation and Metamorphism—South Rinkian FTB

In the Nûkavsak Formation of the south Rinkian FTB, a strong peak in the zircon age data in the 2050–1950 Ma interval defines a typical "Nûkavsak" detrital signature (Kalsbeek et al., 1998; Sanborn-Barrie et al., 2017)—in line with data from the north Rinkian FTB at Holm Ø (Sanborn-Barrie et al., 2017), Kraulshavn (Nuussuaq) (sample 571201), and Qulleqqorsuit (571221). Close to the southern boundary of the PIC, the Nûkavsak Formation is highly deformed and recrystallized and this detrital pattern has been overprinted. In highly recrystallized migmatitic paragneiss from near the lower boundary of the complex (561214), all the zircon grains were interpreted as metamorphic. Most ages belong to the 1900–1850 Ma interval with a smaller peak at ca. 1830 Ma. The PIC was emplaced at ca. 1900–1870 Ma, and therefore the results imply that the complex and its host rocks were deformed together, soon after its intrusion. The metamorphic age is similar to the 1900–1875 Ma age of early deformation (D_1) and high-grade metamorphism in the north Rinkian FTB. Grains with ages at ca. 1830–1820 Ma (560205) we interpret as metamorphic grains recrystallized during D_2. They correspond to the age of peak metamorphism here and in the north Rinkian FTB. These events pre-date the suite of late tectonic leucocratic granites emplaced at ca. 1830–1810 Ma below the lower contact of the PIC (Guarnieri et al., 2022c).

EVOLUTION OF THE RINKIAN OROGEN

The Baffin-Rinkian Suture

Schematic cross sections and a map of the West Greenland continental margin restored to Baffin Island illustrate a tectonic model for the Rinkian orogen (Fig. 13). Cross sections were drawn NW-SE (Figs. 13A–13E), transverse to the overall trend of the orogen (Fig. 13F), and show the tectonic relationship between the north Rinkian FTB, the Foxe fold belt, the Rae craton of northern Baffin Island, and Paleoproterozoic plutonic suites exposed on present-day Baffin Island and Greenland (cf. Corrigan et al., 2009; Whalen et al., 2010; Wodicka et al., 2014; Partin et al., 2014). In map view (Fig. 13F), we link linear belts of magmatic arc plutons on Baffin Island (Qikiqtarjuaq suite, ca. 1.90–1.88 Ga; Cumberland batholith, ca. 1.86–1.84 Ga; and Narsajuaq suite, ca. 1.83–1.82 Ga) (Sanborn-Barrie et al., 2017) and the ca. 1.90–1.85 Ga PIC with a line representing a former subduction boundary: the Baffin-Rinkian suture. Subduction of oceanic lithosphere took place at this boundary over at least 130 m.y. between ca. 1.95 Ga and 1.82 Ga. The orientation of the Baffin-Rinkian suture in northern West Greenland is constrained by the trends of: (1) F_2 fold nappes; (2) the granulite facies hypersthene-in isograd; (3) the leucocratic sill complex; and (4) the PIC magmatic arc (Fig. 3). In northern West Greenland, the WSW-WNW tectonic transport direction inferred for D_1 and D_2 is at a high angle to this former subduction boundary. Subduction was ended after ca. 1.82 Ga and before ca. 1.81 Ga by the arrival of the Rae craton of Baffin Island at this subduction boundary, an event signaled in the north Rinkian FTB by deformation in the Tussaaq shear zone (D_4) and emplacement of the last (post-tectonic) stitching intrusions (late leucocratic granites) at 1813 ± 3 Ma. Deformation during D_3-D_4 (NW-SE shortening) and D_5 (left-lateral heterogeneous shear) may be a consequence of a component of oblique convergence, pre- and syn-collision, at the plate boundary (Fig. 13F). In this model, the Piling Group basin on Baffin Island (Fig. 1B) is a lower-plate basin evolved from an intracontinental rift basin into a foreland basin receiving detritus from the Rinkian FTB, including that from eroded magmatic arc plutons emplaced in the upper plate of the subduction boundary (Fig. 13). According to Partin et al. (2014), the lower part of the Piling Group was deposited in an epicontinental setting before onset of deposition in a pro-foreland basin consistent with a lower-plate setting, matching the model presented here.

Formation and Inversion of the Karrat Group Basin

The lower Karrat Group was deposited in a back-arc basin of Paleoproterozoic age that succeeded continental rift basins of likely Neoarchean age (Fig. 13A). Deposition in the Neoarchean-age basins ended by ca. 2.6 Ga, and deposition of the lower Karrat Group by ca. 2.0–1.95 Ga. Deposition of the lower part of the overlying Nûkavsak Formation may have continued in the marginal basin setting after ca. 1.95 Ga, although phases of inversion may well have affected the Karrat Group basin before this time (Grocott and McCaffrey, 2017). The broad spectrum of zircon ages from the back-arc basin sequence are from grains derived from eroding magmatic arc plutonic rocks, presumably emplaced at the edge of the Neoarchean continent during subduction between ca. 2.6 Ga and 2.0 Ga (Fig. 13B). Neoarchean sedimentary rocks are preserved as the Qeqertarssuaq Formation (Fig. 13A), and overlying back-arc or marginal basin sedimentary rocks (Fig. 13B) are preserved as the Qaarsukassak Formation in the north Rinkian FTB and as the Qaarsukassak, Kangilleq, and Mârmorilik Formations in the south Rinkian FTB (Grocott and McCaffrey, 2017; Guarnieri and Baker, 2022). Paleoproterozoic-age detritus in the northwestern part of the present-day Qaarsukassak Formation outcrop and its relative paucity to the southeast implies polarity with a magmatic arc to the north and west and a continental margin to the south and east (Fig. 13B), consistent with the location of the Rinkian foreland to the east (Grocott and McCaffrey, 2017; Guarnieri and Baker, 2022).

At some time between ca. 1.95 Ga and 1.9 Ga, the subduction boundary advanced to the southeast, and magmatic arc plutons with an age between ca. 2.0 Ga and 1.95 Ga were exhumed and eroded, shedding sediment into the retro- and pro-arc basins (Nûkavsak Formation in the retro-arc basin, Piling Group in the pro-arc basin) (Fig. 13C). At the same time, the active magmatic arc migrated toward the continental margin (foreland), and at ca. 1.9 Ga, the first intrusions of the PIC magmatic arc were emplaced into the base of the Nûkavsak Formation (Fig. 13C). This separated the former back-arc basin into fore- and back-arc domains on either side of the PIC. The setting mirrors the Andean orogen during Late Cretaceous to early Cenozoic time when the magmatic arc migrated ~150 km east to its present location in the Western Cordillera, leaving a Jurassic to Early Cretaceous back-arc basin outboard of the active magmatic arc (Armijo et al., 2015). In the Andes, shortening in the upper plate and emplacement of plutonic complexes in the upper crust accompanied arc migration and, as the subduction boundary advanced toward the continent, led to orogenic uplift of the Coastal Cordillera (Grocott and Taylor, 2002; Grocott et al., 2009) and, subsequently, the Cordillera de Domeyko (Mpodozis and Cornejo, 2012).

In the Rinkian orogen, between ca. 1.9 Ga and ca. 1.82 Ga, the Karrat Group basin on both sides of the PIC was inverted. The sedimentary rocks were metamorphosed and syn-tectonic intrusive units of the PIC were thrust first to the E or SE (D_1) in the Karrat Fjord thrust system and then to the WSW on a ductile thrust system now preserved as a zone of migmatitic paragneiss (D_2) below the PIC (Fig. 13D). The orogenic structure envisaged is a crustal-scale pop-up characterized by bivergent thrusting analogous to the formation of the Cordillera de Domeyko and the Western and Eastern Cordilleras in the present-day northern Andes (Russo and Silver, 1996; Amilibia et al., 2008; Armijo et al., 2015).

In the north and south Rinkian FTB, extensive partial melting and the formation of a granulite facies migmatite complex were taking place at ca. 1.83 Ga, during D_2, with emplacement of an associated (garnet) (cordierite) leucocratic granite sill complex at the base of the PIC between ca. 1.83 Ga and 1.82 Ga, during D_2-D_3 (Fig. 13D). Before ca. 1.81 Ga, continental crust of the lower plate entered the subduction system, and deformation eventually became focused in a ductile shear zone (Tussaaq shear zone) characterized by thrusting to the

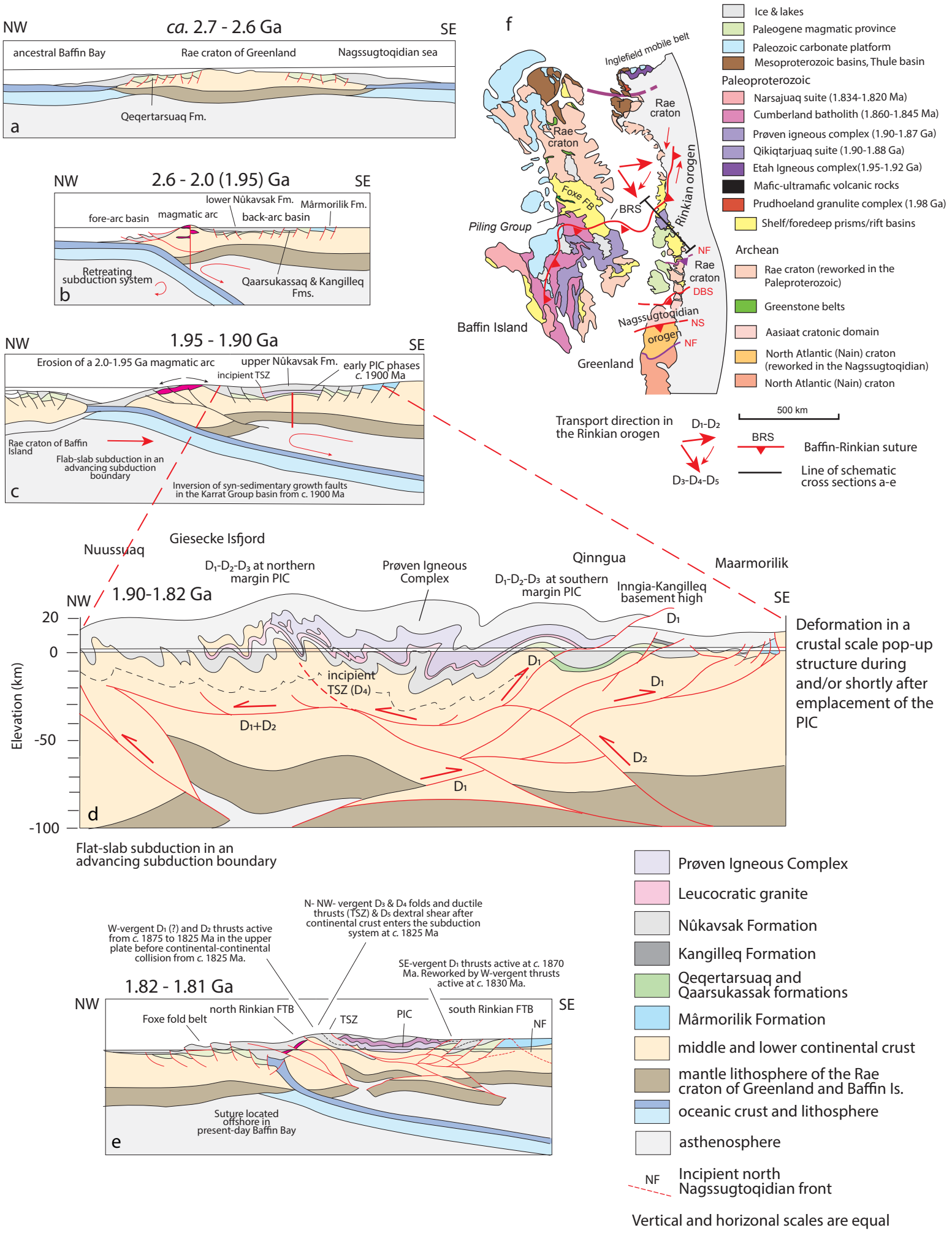

Deformation in a crustal scale pop-up structure during and/or shortly after emplacement of the PIC

Figure 13. Structural and tectonic evolution of the north Rinkian fold-thrust belt (FTB). (A) 2.7–2.6 Ga: Neoarchean to early Paleoproterozoic rifted margins. (B) 2.6–1.95 Ga: Retreating subduction boundary and deposition of the lower Karrat Group in a back-arc basin. (C) 1.95–1.90 Ga: Advancing subduction boundary, erosion of 2.6–1.95 magmatic arcs, deposition of upper Nûkavsak Formation, and emplacement of earliest Prøven Igneous Complex (PIC) units at ca. 1.9 Ga. TSZ—Tussaaq shear zone. (D) 1.90–1.825 Ga: Emplacement and deformation of the main intrusive complexes in the PIC, inversion of back- and fore-arc basins, thrusting to the W to WSW during D_1-D_2 progressive deformation in the north Rinkian FTB, thrusting to the SE (D_1) and then to the W-WNW (D_2) in the south Rinkian FTB, and uplift of the PIC in a bivergent thrust system rooting at the Moho. (E) 1.82–1.81 Ga: Collision between the Rae craton of Baffin Island and the Rae craton of Greenland, NW-SE shortening in the Rinkian FTB and tightening of the structures on the NW-vergent Tussaaq shear zone, and emplacement of late leucocratic granites (stitching intrusions). (F) Map of Baffin Island restored to northern West Greenland showing the continuation of the main tectonic zones from Baffin Island into Greenland. Displacement vectors for the lower plate were first WSW-ENE (D_1-D_2) and later NW-SE (D_3-D_4-D_5), corresponding to a strike-slip component in the Greenland margin. Line of the schematic cross sections (A–E) is shown, perpendicular to the general trend of the Baffin-Rinkian suture. BRS—Baffin-Rinkian suture; T—Thule Basin; FB—Fold belt; NS—Nagssugtoqidian front; DBS—Disko Bugt Suture; NS—Nagssugtoqidian suture; NF—Nagssugtoqidian Front.

NW (D_4) (Fig. 13E). High-temperature deformation in the north Rinkian FTB finds an analogue in zones of bright reflectivity resolved in seismic imaging of the Andean mid-crust interpreted as evidence of widespread anatexis linked to the position of major faults linking upper-crustal fault systems with mid- and deep-crustal faults rooting into detachments at the base of the lithosphere (Oncken et al., 2003; cf. Figs. 13D and 13E).

In the Rinkian orogen, the subduction boundary—the assumed suture zone formed by continental collision—that drove deformation and thermal events at ca. 1.9–1.81 Ga may be located to the west, offshore, in crust attenuated by Cenozoic extension in Baffin Bay (Fig. 13E). However, the location of the continuation of the suture to the north is problematic because a north trend offshore through present-day Baffin Bay would eventually place the boundary remote from exposed magmatic arc rocks of appropriate age in the Greenland margin. It is conceivable that the inferred suture between the Rae craton of Baffin Island and the Rae craton of Greenland is located *onshore* north of the Tussaaq shear zone but is cryptic due to partial subduction of the lower-plate continental margin following continental collision, so there are no rocks representing oceanic lithosphere at the present-day exposure level (Fig. 13E). This solution is consistent with the position and trend of the ca. 1.9–1.85 Ga magmatic arcs exposed on Baffin Island and in Greenland, the WSW-ESE transport direction, the NNW structural trend lines in the north Rinkian FTB, and the trend of metamorphic isograds in the Greenland margin. This is our preferred solution and is supported by a change in the age range of orthogneisses in the Rae craton which are younger to the north of Ryder Isfjord (~74°N) in the north Rinkian FTB (Fig. 3) (Thrane, 2021).

CONCLUSIONS

The Rinkian FTB is an orogenic belt in its own right rather, than a north-vergent syn-collisional fold belt in the lower plate of the Nagssugtoqidian orogen. An orogenic suture—the Baffin-Rinkian suture—separates the Rae craton into at least two Archean segments that were not amalgamated before the Paleoproterozoic. The upper plate of the Rinkian orogen—the Rae craton of southeastern Baffin Island and central West Greenland—comprises four tectonic zones: (1) a foreland to the southeast; (2) a back-arc basin containing the Karrat Group that succeeded a rift system in a Neoarchean continent; (3) a continental magmatic arc—the PIC; and (4) a forearc–accretionary prism–suture zone. The Rinkian lower plate—the Rae craton of northwestern Baffin Island and northern West Greenland—comprises: (1) a lower-plate basin evolved from an intracontinental rift basin into a foreland basin and (2) a post-collisional successor sedimentary basin. It is likely that the Rinkian orogenic suture in western Greenland is blind and located either in the northern West Greenland continental margin, north of Upernavik, or offshore in the Melville Bugt. The trend of the Rinkian orogen is generally NE-SW, and the upper-plate tectonic zones identified in northern West Greenland have along-strike counterparts in Baffin Island.

The structural and metamorphic history of the upper plate of the Rinkian orogen has similarities to the post-Cretaceous evolution of the Andes. In particular, shortening in the upper plate of both orogens led to bivergent thrusting at a high angle to the orogenic trend and the development of characteristic crustal-scale pop-up structures. This deformation inverted the back-arc basins in both orogens, and at the same time, contemporary magmatic arcs migrated into the former back-arc basin and toward the continental margin (foreland), redefining the retro- and pro-arc domains.

The Rinkian back-arc basin was inverted at or soon after ca. 1.9 Ga, at about the same time as the earliest units in the PIC were emplaced, and by ca. 1.875 Ga, Neoarchean and early Paleoproterozoic sedimentary rocks had been metamorphosed during D_1 thrusting at upper amphibolite facies grade. Metamorphism and deformation with peak temperatures at ca. 1.83 Ga during D_2 was at higher grade with widespread anatexis. Deformation (D_3-D_4-D_5) was completed by ca. 1.81 Ga, and there is evidence of only limited partial melting after that time. A continuum of monazite ages between ca. 1.9 Ga and ca. 1.8 Ga implies that deformation and metamorphism, though separated into discrete events, may have been more-or-less continuous throughout this period. Extensive partial melting of the Rinkian crust also finds an Andean analogue in the well characterized "bright spots" resolved in the mid-crust by seismic reflection surveys of the Andes.

ACKNOWLEDGMENTS

Our research over two decades has been supported by: Avannaa Resources Ltd., the Carlsberg Fund, Durham University, the Geological Survey of Denmark and Greenland (GEUS), the Ion Microprobe Facility at Stockholm University (NORDSIM), the Ministry of Mineral Resources of Greenland (MMR), the UK Natural Environment Research Council (GR3/12070), the Dr. Schürmann Foundation, and the Royal Society of London. We would like to thank our collaborators at GEUS and Durham University, particularly Thomas Kokfelt, Erik Sørensen, Diogo Rosa, Nigel Baker, and Bob Holdsworth; they have contributed immensely to the development of our ideas. The review panel at *Geosphere*—Dawn Kellett, Bob Miller, and Rob Strachan—have substantially improved the presentation of our work. We sincerely thank you all. This paper is dedicated to the memory of Reinoud Vissers and T.C.R. (Chris) Pulvertaft—our friends and colleagues.

REFERENCES CITED

Alsop, G.I., and Holdsworth, R.E., 1999, Vergence and facing patterns in large-scale sheath folds: Journal of Structural Geology, v. 21, p. 1335–1349, https://doi.org/10.1016/S0191-8141(99)00099-1.

Alsop, G.I., and Holdsworth, R.E., 2002, The geometry and kinematics of flow perturbation folds: Tectonophysics, v. 350, p. 99–125, https://doi.org/10.1016/S0040-1951(02)00084-7.

Alsop, G.I., and Holdsworth, R.E., 2004, The geometry and topology of natural sheath folds: A new tool for structural analysis: Journal of Structural Geology, v. 26, p. 1561–1589, https://doi.org/10.1016/j.jsg.2004.01.009.

Amilibia, A., Sàbat, F., McClay, K.R., Muñoz, J.A., Roca, E., and Chong, G., 2008, The role of inherited tectono-sedimentary architecture in the development of the central Andean mountain belt: Insights from the Cordillera de Domeyko: Journal of Structural Geology, v. 30, p. 1520–1539, https://doi.org/10.1016/j.jsg.2008.08.005.

Armijo, R., Lacassin, R., Coudurier-Curveur, A., and Carrizo, D., 2015, Coupled tectonic evolution of Andean orogeny and global climate: Earth-Science Reviews, v. 143, p. 1–35, https://doi.org/10.1016/j.earscirev.2015.01.005.

Connelly, J.N., and Thrane, K., 2005, Rapid determination of Pb isotopes to define Precambrian allochthonous domains: An example from West Greenland: Geology, v. 33, p. 953–956, https://doi.org/10.1130/G21720.1.

Connelly, J.N., van Gool, J.A.M., and Mengel, F.C., 2000, Temporal evolution of a deeply eroded orogen: the Nagssugtoqidian Orogen, West Greenland: Canadian Journal of Earth Sciences, v. 37, p. 1121–1142, https://doi.org/10.1139/e00-032.

Connelly, J.N., Thrane, K., Krawiec, A.W., and Garde, A.A., 2006, Linking the Palaeoproterozoic Nagssugtoqidian and Rinkian orogens through the Disko Bugt region of West Greenland: Journal of the Geological Society, v. 163, p. 319–335, https://doi.org/10.1144/0016-764904-115.

Corrigan, D., Pehrsson, N., Wodicka, N., and de Kemp, E., 2009, The Palaeoproterozoic Trans-Hudson Orogen: A prototype of modern accretionary processes, *in* Murphy, J.B., Keppie, J.D., and Hynes, A.J., eds., Ancient Orogens and Modern Analogues: Geological Society, London, Special Publication 327, p. 457–479, https://doi.org/10.1144/SP327.19.

Escher, A., and Burri, M., 1967, Stratigraphy and structural development of the Precambrian rocks in the area north-east of Disko Bugt, West Greenland: Geological Survey of Greenland Report 13, 28 p., https://doi.org/10.34194/rapggu.v13.7161.

Escher, A., and Pulvertaft, T.C.R., 1976, Rinkian mobile belt of West Greenland, *in* Escher, A. and Watt, W.S., eds., Geology of Greenland: Copenhagen, Geological Survey of Greenland, p. 105–119.

Escher, J.C., compiler, 1981, Geologisk kort over Grønland, 1:100 000 Tasiussaq 73 V.1 Syd: Copenhagen, Grønlands Geologiske Undersøgelse.

Escher, J.C., compiler, 1983a, Geologisk kort over Grønland, 1:100 000 Ussing Isfjord 73 V.1 Nord: Copenhagen, Grønlands Geologiske Undersøgelse.

Escher, J.C., compiler, 1983b, Geologisk kort over Grønland, 1:100 000 Kuvdlorssuaq 74 V.1 Nord/Syd: Copenhagen, Grønlands Geologiske Undersøgelse.

Escher, J.C., compiler, 1995a, Geologisk kort over Grønland, 1:100 000 Ataa 69 V.3 Nord: Copenhagen, Grønlands Geologiske Undersøgelse.

Escher, J.C., compiler, 1995b, Geologisk kort over Grønland, 1:500 000 Upernavik Isfjord Sheet 4: Copenhagen, Grønlands Geologiske Undersøgelse.

Escher, J.C., and Stecher, O., 1978, Precambrian geology of Upernavik–Red Head region (72°15′–75°15′N), northern West Greenland, *in* Report of Activities, 1977: Geological Survey of Greenland Report 90, p. 23–26, https://doi.org/10.34194/rapggu.v90.7582.

Escher, J.C., and Stecher, O., 1980, Field work on Precambrian granites and metasediments in the Søndre Upernavik–Kuvdlorssuaq region (72°00′–74°40′N), *in* Report of Activities, 1979: Geological Survey of Greenland Report 100, p. 38–41, https://doi.org/10.34194/rapggu.v100.7692.

Garde, A.A., 1978, The lower Proterozoic Marmorilik Formation, east of Mârmorilik, West Greenland: Meddelelser om Grønland, v. 200, no. 3, p. 1–71.

Garde, A.A., compiler, 1994, Precambrian geology between Qarajaq Isfjord and Jakobshvn Isfjord, West Greenland: Geologisk kort over Grønland, 1:250 000 Nûgâtsiaq 71 V.2 Nord: Copenhagen, Grønlands Geologiske Undersøgelse.

Garde, A.A., and Hollis, J.A., 2010, A buried Paleoproterozoic spreading ridge in the northern Nagssugtoqidian orogen, West Greenland, *in* Kusky, T.M., Zhai, M.G., and Xiao, W., eds., The Evolving Continents: Understanding Processes of Continental Growth: Geological Society of London Special Publication 338, p. 213–234, https://doi.org/10.1144/SP338.11.

Garde, A.A., and Pulvertaft, T.C.R., 1976, Age relations of the Precambrian Mârmorilik Marble Formation, central West Greenland, *in* Report of Activities, 1975: Geological Survey of Greenland Report 80, p. 49–53, https://doi.org/10.34194/rapggu.v80.7483.

Garde, A.A., and Steenfeldt, A., 1999, Precambrian geology of Nuussuaq and the area north-east of Disko Bugt, West Greenland, *in* Kalsbeek, F., ed., Precambrian Geology of the Disko Bugt Region, West Greenland: Geology of Greenland Survey Bulletin 181, p. 6–40, https://doi.org/10.34194/ggub.v181.5108.

GEUS (Geological Survey of Denmark and Greenland), 2022, Greenland Stratigraphic Database: GEUS Dataverse, V1, https://doi.org/10.22008/FK2/F9MBNJ.

Grocott, J., and Davis, S.C., 1999, Deformation at the southern boundary of the late Archean Atâ tonalite and the extent of Proterozoic reworking of the Disko terrane, West Greenland, *in* Kalsbeek, F., ed., Precambrian Geology of the Disko Bugt Region, West Greenland: Geology of Greenland Survey Bulletin 181, p. 155–169, https://doi.org/10.34194/ggub.v181.5123.

Grocott, J., and McCaffrey, K.J.W., 2017, Basin evolution and destruction in an Early Proterozoic continental margin: The Rinkian fold-thrust belt of central West Greenland: Journal of the Geological Society, v. 174, p. 453–467, https://doi.org/10.1144/jgs2016-109.

Grocott, J., and Pulvertaft, T.C.R., 1990, The Early Proterozoic Rinkian belt of central West Greenland, *in* Lewry, J.F. and Stauffer, M.R., eds., The Early Proterozoic Trans-Hudson Orogen of North America: Geological Association of Canada Special Paper 37, p. 443–463.

Grocott, J., and Taylor, G.K., 2002, Magmatic arc fault systems, deformation partitioning and emplacement of granitic complexes in the Coastal Cordillera, north Chilean Andes (25°30′S to 27°00′S): Journal of the Geological Society, v. 159, p. 425–443, https://doi.org/10.1144/0016-764901-124.

Grocott, J., and Vissers, R.L.M., 1984, Field mapping of the early Proterozoic Karrat Group on Svartenhuk Halvø, central West Greenland, *in* Report of Activities, 1983: Geological Survey of Greenland Report 120, p. 25–31, https://doi.org/10.34194/rapggu.v120.7853.

Grocott, J., van den Eeckhout, B., and Vissers, R.L.M., 1987, Mantled gneiss antiforms and fold nappes in the Rinkian belt, West Greenland: Diapiric structures or structures formed in a thrust system?: Journal of the Geological Society, v. 144, p. 723–734, https://doi.org/10.1144/gsjgs.144.5.0723.

Grocott, J., Arévalo, C., Welkner, D., and Cruden, A., 2009, Fault-assisted vertical pluton growth: Coastal Cordillera, north Chilean Andes: Journal of the Geological Society, v. 166, p. 295–301, https://doi.org/10.1144/0016-76492007-165.

Guarnieri, P., and Baker, N., 2022, Tectonic inversion of listric normal faults in the foreland of the Rinkian Orogen (Maarmorilik, central West Greenland: Journal of Structural Geology, v. 159, https://doi.org/10.1016/j.jsg.2022.104598.

Guarnieri, P., Partin, C.A., and Rosa, D., 2016, Palaeovalleys at the basal unconformity of the Paleoproterozoic Karrat Group, West Greenland: Geological Survey of Denmark and Greenland Bulletin, v. 35, p. 63–66, https://doi.org/10.34194/geusb.v35.4940.

Guarnieri, P., Baker, N., Rosa, D., and Sørensen, E.V., 2022a, Geological map of Greenland 1:100 000, Maarmorilik 71 V. 2 Syd: Copenhagen, Geological Survey of Denmark and Greenland, https://doi.org/10.22008/FK2/07OYKX.

Guarnieri, P., Baker, N., Rosa, D., and Sørensen, E.V., 2022b, Geological map of Greenland 1:100 000, Nugaatsiaaq 71 V. 2 Nord: Copenhagen, Geological Survey of Denmark and Greenland, https://doi.org/10.22008/FK2/PGSMJH.

Guarnieri, P., Baker, N., Rosa, D., and Sørensen, E.V., 2022c, Geological map of Greenland 1:100 000, Pannertooq 7 V. 2 Syd: Copenhagen, Geological Survey of Denmark and Greenland.

Guarnieri, P., Rosa, D., Thrane, K., Kokfelt, T.F., Sørensen, E.V., and Baker, N., 2022d, Paleoproterozoic Cordilleran-type tectonics in central West Greenland: Abstract EGu22-13531 presented at European Geosciences Union General Assembly 2022, Vienna, Austria, 23–27 May, https://doi.org/10.5194/egusphere-egu22-13531.

Henderson, G., 1969, The use of structural contour maps in the study of gneiss-metasediment relations in the Umanak area, West Greenland: Geological Association of Canada Special Paper 5, p. 129–142.

Henderson, G., and Pulvertaft, T.C.R., 1967, The stratigraphy and structure of the Precambrian rocks of the Umanak area, West Greenland: Meddelelser fra Dansk Geologisk Forening, v. 17, p. 1–20.

Henderson, G., and Pulvertaft, T.C.R., 1987, Lithostratigraphy and structure of a Lower Proterozoic dome and nappe complex: Descriptive text for geological map of Greenland 1:100 000-scale sheets Mârmorilik 71 V.2 Syd, Nûgâtsiaq 71 V.2 Nord, Pangnertôq 72 V.2 Syd: Copenhagen, Geological Survey of Greenland.

Henderson, J.R., 1981, Structural analysis of sheath folds with horizontal *X*-axes, northeast Canada: Journal of Structural Geology, v. 3, p. 203–210, https://doi.org/10.1016/0191-8141(81)90016-X.

Henderson, J.R., Grocott, J., Henderson, M.N., and Perreault, S., 1989, Tectonic history of the Lower Proterozoic Foxe-Rinkian Belt in central Baffin Island, N.W.T, *in* Current Research, Part C: Canadian Shield: Geological Survey of Canada Paper 89-1C, p. 186–197, https://doi.org/10.4095/126852.

Higgins, A.K., and Soper, N.J., 1999, The Precambrian supracrustal rocks of Nunataq, north-east of Disko Bugt, West Greenland, *in* Kalsbeek, F., ed., Precambrian Geology of the Disko Bugt Region, West Greenland: Geology of Greenland Survey Bulletin 181, p. 79–86, https://doi.org/10.34194/ggub.v181.5116.

Hoffmann, P.F., 1999, Dynamics of the tectonic assembly of northeast Laurentia in geon 18 (1.9–1.8 Ga): Geoscience Canada, v. 17, p. 222–226.

Kalsbeek, F., 1981, The northward extent of the Archean basement of Greenland—A review of Rb-Sr whole-rock ages: Precambrian Research, v. 14, p. 203–219, https://doi.org/10.1016/0301-9268(81)90039-5.

Kalsbeek, F., Pidgeon, R.T., and Taylor, P.N., 1987, Nagssugtoqidian mobile belt of West Greenland: A cryptic 1850 Ma suture between two Archean continents—Chemical and isotopic evidence: Earth and Planetary Science Letters, v. 85, p. 365–385, https://doi.org/10.1016/0012-821X(87)90134-8.

Kalsbeek, F., Pulvertaft, T.C.R., and Nutman, A., 1998, Geochemistry, age and origin of metagreywackes from the Paleoproterozoic Karrat Group, Rinkian Belt, West Greenland: Precambrian Research, v. 91, p. 383–399, https://doi.org/10.1016/S0301-9268(98)00059-X.

Larsen, J.G., and Grocott, J., compilers, 1991, Geologisk kort over Grønland, 1:100 000 Svartenhuk 71 V.1 Nord: Copenhagen, Grønlands Geologiske Undersøgelse, https://doi.org/10.22008/FK2/KMAG0B.

Lewry, J.F., and Stauffer, M.R., eds., 1990, The Early Proterozoic Trans-Hudson Orogen of North America: Geological Association of Canada Special Paper 37, 505 p.

Lundin, E.R., and Doré, A.G., 2019, Non-Wilsonian break-up predisposed by transforms: Examples from the North Atlantic and Arctic, *in* Wilson, R.W., Houseman, G.A., McCaffrey, K.J.W., Doré, A.G., and Buiter, S.J.H., eds., Fifty Years of the Wilson Cycle Concept in Plate Tectonics: Geological Society, London, Special Publication 470, p. 375–392, https://doi.org/10.1144/SP470.6.

Mpodozis, C., and Cornejo, P., 2012, Cenozoic tectonics and porphyry copper systems of the Chilean Andes, *in* Hedenquist, J.W., Harris, M., and Camus, F., eds., Geology and Genesis of Major Copper Deposits and Districts of the World: A Tribute to Richard H. Sillitoe: Society of Economic Geologists Special Publication 16, p. 329–360.

Nutman, A.P., and Kalsbeek, F., 1999, SHRIMP U-Pb zircon ages for Archean granitoid rocks, Ataa area, north-east Disko Bugt, West Greenland, *in* Kalsbeek, F., ed., Precambrian Geology of the Disko Bugt Region, West Greenland: Geology of Greenland Survey Bulletin 181, p. 49–54.

Nutman, A.P., Dawes, P.R., Kalsbeek, F., and Hamilton, M.A. 2008, Palaeoproterozoic and Archaean gneiss complexes in northern Greenland: Palaeoproterozoic terrane assembly in the high Arctic: Precambrian Research, v.161, p. 419–451, https://doi.org/10.1016/j.precamres.2007.09.006.

Oncken, O., Asch, G., Haberland, C., Metchie, J., Sobolev, S., Stiller, M., Yuan, X., Brasse, H., Buske, S., Giese, P., Görze, H.-J., Lueth, S., Scheuber, E., Shapiro, S., Wigger, P., Yoon, M.-K., Bravo, P., Vieytes, H., Chong, G., Gonzales, G., Wilke, H.-G., Lüschen, E., Martinez, E., Rössling, R., Ricaldi, E., and Rietbrock, A., 2003, Seismic imaging of a convergent continental margin and plateau in the central Andes (Andean Continental Research Project 1996 (ANCORP'96)): Journal of Geophysical Research, v. 108, 2328, https://doi.org/10.1029/2002JB001771, correction available at https://doi.org/10.1029/2006JB004431.

Partin, C.A., Bekker, A., Corrigan, D., Modeland, S., Francis, D., and Davis, D.W., 2014, Sedimentological and geochemical basin analysis of the Paleoproterozoic Penrhyn and Piling groups of Arctic Canada: Precambrian Research, v. 251, p. 80–101, https://doi.org/10.1016/j.precamres.2014.06.010.

Pulvertaft, T.C.R., 1973, Recumbent folding and flat-lying structure in the Precambrian of northern West Greenland: Philosophical Transactions of the Royal Society of London, Series A: Mathematical and Physical Sciences, v. 273, p. 535–545.

Pulvertaft, T.C.R., 1986, The development of thin thrust sheets and basement-cover sandwiches in the southern part of the Rinkian belt, Umanak district, West Greenland, *in* Developments in Greenland Geology: Geological Survey of Greenland Report 128, p. 75–87, https://doi.org/10.34194/rapggu.v128.7926.

Pulvertaft, T.C.R., Escher, J.C., and Stecher, O., 1979, Map of field observations, Upernavik 72 V1 Nord at 1:40000-scale: Geological Survey of Denmark and Greenland Archive File S412-14.

Ramsay, J.G., and Huber, M.I., 1987, The Techniques of Modern Structural Geology, Volume 2: Folds and Fractures: London, Academic Press Ltd., 700 p.

Rosa, D., Guarnieri, P., Hollis, J., Kolb, J., Partin, C., Petersen, J., Sørensen, E.V., Thomassen, B., Thomsen, L., and Thrane, K., 2016, Architecture and mineral potential of the Paleoproterozoic Karrat Group, West Greenland: Results of the 2015 season: Geological Survey of Denmark and Greenland Report 2016/12, 98 p., https://doi.org/10.22008/gpub/30756.

Rosa, D., DeWolfe, M., Guarnieri, P., Kolb, J., LaFlamme, C., Partin, C., Salahi, S., Sørensen, E.V., Thaarup, S., Thrane, K., and Zimmermann, R., 2017, Architecture and mineral potential of the Paleoproterozoic Karrat Group, West Greenland: Results of the 2016 season: Geological Survey of Denmark and Greenland Report 2017/5, 112 p., https://doi.org/10.22008/gpub/32501.

Rosa, D., Bernstein, S., DeWolfe, M., Dziggel, A., Grocott, J., Guarnieri, P., Kolb, J., Partin, C.A., Sørensen, E.V., and Zimmermann, R., 2018, Architecture and mineral potential of the Paleoproterozoic Karrat Group, West Greenland: Results of the 2017 season: Geological Survey of Denmark and Greenland Report 2018/23, 102 p., https://doi.org/10.22008/gpub/32569.

Russo, R.M., and Silver, P.G., 1996, Cordillera formation, mantle dynamics, and the Wilson cycle: Geology, v. 24, p. 511–514, https://doi.org/10.1130/0091-7613(1996)024<0511:CFMDAT>2.3.CO;2.

Sanborn-Barrie, M., Thrane, K., Wodicka, N., and Rayner, N., 2017, The Laurentia–West Greenland connection at 1.9 Ga: New insights from the Rinkian fold belt: Gondwana Research, v. 51, p. 289–309, https://doi.org/10.1016/j.gr.2017.07.002.

Sawyer, E.W., 2008, Atlas of Migmatites: The Canadian Mineralogist Special Publication 9, 371 p.

Sleath, P.R., 2021, Tectonic evolution of the Prøven Igneous Complex within the Rinkian fold-thrust belt, West Greenland: Investigation using 3D photogrammetry [M.S. thesis]: Durham, UK, Durham University, Department of Earth Sciences, 113 p.

Sørensen, E.V., and Dueholm, M., 2018, Analytical procedures for 3D mapping at the Photogeological Laboratory of the Geological Survey of Denmark and Greenland: Geological Survey of Denmark and Greenland Bulletin, v. 41, p. 99–104, https://doi.org/10.34194/geusb.v41.4353.

Sørensen, E.V., and Guarnieri, P., 2018, Remote geological mapping using 3D photogrammetry: an example from Karrat, West Greenland: Geological Survey of Denmark and Greenland Bulletin, v. 41, p. 63–66, https://doi.org/10.34194/geusb.v41.4343.

St-Onge, M.R., van Gool, J.A.M., Garde, A.A., and Scott, D.J., 2009, Correlation of Archean and Paleoproterozoic units between northeastern Canada and western Greenland: Constraining the pre-collisional upper plate accretionary history of the Trans-Hudson orogen, *in* Cawood, P.A. and Kröner, A., eds., Earth Accretionary Systems in Space and Time: Geological Society, London, Special Publication 318, p. 193–235, https://doi.org/10.1144/SP318.7.

Thrane, K., 2021, The oldest part of the Rae craton identified in western Greenland: Precambrian Research, v. 357, 106139, https://doi.org/10.1016/j.precamres.2021.106139.

Thrane, K., Baker, J., Connelly, J., and Nutman, A., 2005, Age, petrogenesis and metamorphism of the syn-collisional Prøven Igneous Complex, West Greenland: Contributions to Mineralogy and Petrology, v. 149, p. 541–555, https://doi.org/10.1007/s00410-005-0660-0.

van Gool, J.A.M., Connelly, J.N., Marker, M., and Mengel, F.C., 2002, The Nagssugtoqidian Orogen of West Greenland: Tectonic evolution and regional correlations from a West Greenland perspective: Canadian Journal of Earth Sciences, v. 39, p. 665–686, https://doi.org/10.1139/e02-027.

Van Kranendonk, M.J., St-Onge, M.R., and Henderson, J.R., 1993, Paleoproterozoic tectonic assembly of Northeast Laurentia through multiple indentations: Precambrian Research, v. 63, p. 325–347, https://doi.org/10.1016/0301-9268(93)90039-5.

Watt, W.S., compiler, 2019, Stratigraphic Lexicon for Greenland: Nomenclature of Stratified Successions in Current Use: Copenhagen, Geological Survey of Denmark and Greenland, 327 p.

Whalen, J.B., Wodicka, N., Taylor, B.E., and Jackson, G.D., 2010, Cumberland batholith, Trans-Hudson Orogen, Canada: Petrogenesis and implications for Paleoproterozoic crustal and orogenic processes: Lithos, v. 117, p. 99–118, https://doi.org/10.1016/j.lithos.2010.02.008.

Wodicka, N., St-Onge, M.R., Corrigan, D., Scott, D.J., and Whalen, J.B., 2014, Did a proto-ocean basin form along the southeastern Rae cratonic margin? Evidence from U-Pb geochronology, geochemistry (Sm-Nd and whole rock), and stratigraphy of the Paleoproterozoic Piling Group, northern Canada: Geological Society of America Bulletin, v. 126, p. 1625–1653, https://doi.org/10.1130/B31028.1.

Yakymchuk, C., Kirkland, C.L., and Clark, C., 2018, Th/U ratios in metamorphic zircon: Journal of Metamorphic Geology, v. 36, p. 715–737, https://doi.org/10.1111/jmg.12307.